

Alma Mater Studiorum Università di Bologna
Archivio istituzionale della ricerca

Ocean acidification causes variable trait-shifts in a coral species

This is the final peer-reviewed author's accepted manuscript (postprint) of the following publication:

Published Version:

Teixido, N., Caroselli, E., Alliouane, S., Ceccarelli, C., Comeau, S., Gattuso, J.-P., et al. (2020). Ocean acidification causes variable trait-shifts in a coral species. *GLOBAL CHANGE BIOLOGY*, 26(12), 6813-6830 [10.1111/gcb.15372].

Availability:

This version is available at: <https://hdl.handle.net/11585/783806> since: 2024-05-16

Published:

DOI: <http://doi.org/10.1111/gcb.15372>

Terms of use:

Some rights reserved. The terms and conditions for the reuse of this version of the manuscript are specified in the publishing policy. For all terms of use and more information see the publisher's website.

This item was downloaded from IRIS Università di Bologna (<https://cris.unibo.it/>).
When citing, please refer to the published version.

(Article begins on next page)

This is the final peer-reviewed accepted manuscript of:

Núria Teixidó, Erik Caroselli, Samir Alliouane, Chiara Ceccarelli, Steeve Comeau, et al.. Ocean acidification causes variable trait-shifts in a coral species. Global Change Biology, 2020, 26 (12), pp.6813-6830

The final published version is available online at
<https://dx.doi.org/10.1111/gcb.15372>

Rights / License:

The terms and conditions for the reuse of this version of the manuscript are specified in the publishing policy. For all terms of use and more information see the publisher's website.

This item was downloaded from IRIS Università di Bologna (<https://cris.unibo.it/>)

When citing, please refer to the published version.

Ocean acidification causes variable trait shifts in a coral species

Nuria Teixidó^{1,2*}, Erik Caroselli^{3*}, Samir Alliouane ², Chiara Ceccarelli³, Steeve Comeau², Jean-Pierre Gattuso^{2,4}, Pietro Fici³, Fiorenza Micheli^{5,6}, Alice Mirasole¹, Stephen G. Monismith⁷, Marco Munari¹, Stephen R. Palumbi⁵, Elizabeth Sheets⁵, Lidia Urbini⁸, Cinzia De Vittor⁸, Stefano Goffredo^{3,9*}, Maria Cristina Gambi¹

¹Stazione Zoologica Anton Dohrn, Ischia Marine Centre, Punta San Pietro 80077, Ischia, Naples, Italy.

²Sorbonne Université, CNRS, Laboratoire d'Océanographie de Villefranche, 181 chemin du Lazaret, 06230 Villefranche-sur-mer, France.

³Marine Science Group, Department of Biological, Geological, and Environmental Sciences, University of Bologna, Via Selmi 3, 40126 Bologna, Italy.

⁴Institute for Sustainable Development and International Relations, Sciences Po, 27 rue Saint Guillaume, F-75007 Paris, France

⁵Department of Biology, Hopkins Marine Station, Stanford University, Pacific Grove, CA, 93950, USA.

⁶Stanford Center for Ocean Solutions, Pacific Grove, CA, 93950, USA.

⁷Department of Civil and Environmental Engineering, Stanford University, Stanford, CA, 94305, USA.

⁸Istituto Nazionale di Oceanografia e di Geofisica Sperimentale (OGS), Via A. Piccard 54, 34151, Trieste, Italy.

⁹Fano Marine Center, Department of Biological, Geological and Environmental Sciences,

24 University of Bologna, viale Adriatico 1/N, 61032 Fano, Italy

25 *corresponding author. Email: nuria.teixido@obs-vlfr.fr ; erik.caroselli@unibo.it ;

26 s.goffredo@unibo.it

27

For Review Only

Abstract

High $p\text{CO}_2$ habitats and their populations provide an unparalleled opportunity to assess how species may survive under future ocean acidification conditions, and help to reveal the traits that confer tolerance. Here we utilize a unique CO_2 vent system to study the effects of exposure to elevated $p\text{CO}_2$ on trait-shifts observed throughout natural populations of *Astroides calycularis*, an azooxanthellate scleractinian coral endemic to the Mediterranean. Unexpected shifts in skeletal and growth patterns were found. Colonies shifted to a skeletal phenotype characterized by encrusting morphology, smaller size, reduced coenosarc tissue, fewer polyps, and less porous and denser skeletons at low pH. Interestingly, while individual polyps calcified more and extended faster at low pH, whole colonies found at low pH site calcified and extended their skeleton at the same rate as did those at ambient pH sites. Transcriptomic data revealed strong genetic differentiation among local populations of this warm water species whose distribution range is currently expanding northward. We found excess differentiation in the CO_2 vent population for genes central to calcification, including genes for calcium management (calmodulin, calcium-binding proteins), pH regulation (V-type proton ATPase), and inorganic carbon regulation (carbonic anhydrase). Combined, our results demonstrate how coral populations can persist in high $p\text{CO}_2$ environments, making this system a powerful candidate for investigating acclimatization and local adaptation of organisms to global environmental change.

1. INTRODUCTION

Understanding the effects of environmental variability and extremes on natural populations and ecosystems is a key priority as global environmental change intensifies (Bennett, Duarte, Marba, & Wernberg, 2019; Bozinovic, Calosi, & Spicer, 2011). High local variability in physical and chemical ocean properties can create extreme climatic environments, where marine species persist under suboptimal environmental conditions such as highly variable temperatures, marginal habitats at latitudinal extremes, and acidification at CO₂ vent sites (Camp et al., 2018; Kapsenberg & Cyronak, 2019; Kroeker et al., 2019). Populations living in these unique settings experience high environmental variability and can have broad physiological tolerance to environmental stressors that would prevent survival of conspecifics living in less variable micro-environments (Bozinovic et al., 2011; Thomas et al., 2018). Two important mechanisms for intraspecific variation in tolerance to environmental variability and extremes are adjusting life traits through phenotypic plasticity and local adaptation, and these processes may interact synergistically (Hoffmann & Sgro, 2011; Savolainen, Lascoux, & Merilä, 2013). Phenotypic plasticity (also referred to as acclimatization) is the ability of a genotype to produce different morphological and physiological responses when exposed to different environmental conditions within an organism's lifespan, resulting in a phenotypic shift that is plastic and often reversible (Savolainen et al., 2013; Thomas et al., 2018). Adaptation is the result of natural selection on beneficial genotypes in a population where these changes are heritable and passed on to the next generation (Hoffmann & Sgro, 2011; Savolainen et al., 2013). Natural extreme environments are potential locations for climate-adapted populations where, for example, microhabitats experiencing periodic temperature extremes have shown to generate high-tolerance in some reef-building corals (Palumbi, Barshis, Traylor-Knowles, & Bay, 2014; Thomas et al., 2018). However, there is still much to learn about

the underlying mechanisms of acclimatization and adaptation to climate variability and extremes by studying populations in naturally variable environments. Such studies are critical for predicting future biological responses to rapid global environmental change.

Insights into species' tolerance to environmental change may be gained by analyzing traits that directly influence an organism's performance (Mouillot, Graham, Villéger, Mason, & Bellwood, 2013). Shifts in the occurrence of these traits under variable environmental conditions can reflect patterns of differential survival and growth strategies; for example, different morphological forms (*e.g.* massive or encrusting), longevity, size, growth rates, physical defenses and dispersal ability (Darling, Alvarez-Filip, Oliver, Mcclanahan, & Côté, 2012; Teixidó et al., 2018). These traits provide relevant information about life strategies that are the result of different evolutionary and ecological processes and influence, both the fitness of individuals and the viability of natural populations (Darling et al., 2012; Mouillot et al., 2013; Teixidó et al., 2018). However, we still know comparatively little about trait-shifts within natural populations and the capacity to adapt to long-term novel environmental conditions.

Natural volcanic CO₂ vents cause local acidification of seawater and are used as a proxy to study future ocean acidification (Enochs et al., 2015; Fabricius et al., 2011; Hall-Spencer et al., 2008). Ocean acidification reflects a suite of changes in seawater carbonate chemistry due to the uptake of excess anthropogenic CO₂ by the ocean, resulting in a decline in the surface ocean pH, carbonate ion concentration, and saturation state of calcium carbonate minerals (*e.g.* aragonite), while increasing the partial pressure of carbon dioxide ($p\text{CO}_2$) and bicarbonate ion concentrations (Doney, Fabry, Feely, & Kleypas, 2009). Low pH levels in natural CO₂ vents represent future climatic conditions where, relative to 1870, surface pH is projected to decline by -0.14 to -0.4 pH units by 2100, under IPCC Representative Concentration Pathways (RCP) RCP 2.6 (low CO₂

emissions) and RCP 8.5 (high CO₂ emissions) (Fabricius et al., 2011; Gattuso et al., 2015; Goffredo et al., 2014; Teixidó et al., 2018). Although these pH conditions can provide some insight into future acidification scenarios, they are not perfect proxies. One important assumption to consider is that variability of seawater pH increases with decreasing means at CO₂ vent systems. Although variability in pH/*p*CO₂ will increase with dissolved inorganic carbon due to the thermodynamics of the carbonate system in the future ocean (Takeshita et al., 2015), it is not possible to disentangle the effects of changes in the mean versus variability in this system. Thus, the conditions in the pH zones should be considered as pH regimes, with decreases in mean pH coinciding with increases in variability. Nevertheless, these high *p*CO₂ environments and their populations provide an unparalleled opportunity to assess how species may survive into future pH conditions and to reveal if general traits that confer tolerance can be identified.

Corals are key marine organisms that are particularly vulnerable to the impacts of climate change and ocean acidification (Brandl et al., 2019; Gattuso et al., 2015). They create habitats for many species, enhancing biodiversity, playing fundamental ecological roles and sustaining ecosystem processes and services such as fisheries, coastal protection and tourism (Brandl et al., 2019; Gattuso et al., 2015). Ocean acidification may pose a major threat to corals because their growth relies on the precipitation of calcium carbonate (calcification), a process that is expected to decrease as seawater acidity increases (Chan & Connolly, 2013). Studies conducted at CO₂ vent ecosystems on native corals have reported an overall decline in species abundances, decreases in calcification and skeletal density with increasing acidification (Fabricius et al., 2011; Fantazzini et al., 2015; Goffredo et al., 2014).

Here we utilize a unique CO₂ vent system to investigate the effects of exposure to elevate *p*CO₂ on trait-shifts on *Astroides calycularis*, an azooxanthellate scleractinian coral endemic to the

117 Mediterranean, that naturally occurs in the acidified environment of a newly discovered CO₂ vent
118 system in Ischia, Italy. This CO₂ vent system locally acidifies the seawater with gas comprising
119 92-95% CO₂ (no sulphur, and no temperature anomaly). *A. calycularis* is a long-lived coral (large
120 colonies may have a life span of several decades), considered a warm-water species with a narrow
121 temperature tolerance confined to 14°C during winter (Bianchi, 2007; Zibrowius, 1995). *A.*
122 *calycularis* has low dispersal capacities, and therefore restricted gene flow (Casado-Amezúa,
123 Goffredo, Templado, & Machordom, 2012). Because *A. calycularis* is a calcifying and long-lived
124 species with low dispersal capacity, and found throughout the CO₂ vents, it is a great model system
125 for investigating variation in local climate phenotypic plasticity and adaptation. Previous research
126 on the effects of ocean acidification on *A. calycularis* has shown contrasting results: a reduction
127 of net calcification rates was found when colonies growing in ambient pH conditions were
128 transplanted to a vent system with pH below 7.7 (Prada et al., 2017), while no change in
129 calcification under acidification was observed in controlled laboratory conditions (Movilla et al.,
130 2016). We compare populations living near the vent to two reference areas outside the influence
131 of CO₂ venting to examine the effects of low pH conditions on *A. calycularis* traits, to characterize
132 the genetic population structure, and to identify differentiation in genes that are central to
133 calcification. Specifically, we addressed the following questions: i) do populations at the CO₂ vent
134 and reference sites exhibit significant trait variation?, ii) do these nearby populations display
135 genetic differentiation?, and iii) does the CO₂ vent population have highly divergent SNP
136 genotypes from calcium- related loci? To answer these questions, we characterized the physical
137 and chemical parameters of the study sites and combined *in situ* population demographics, skeletal
138 characteristics, computed tomography and transcriptomic approaches to assess changes in
139 population abundance, skeletal properties, age, and genomics of differentiation of *A. calycularis*.

2. MATERIAL AND METHODS

2.1 Experimental design and study sites

Here we compare natural populations of the scleractinian coral *A. calycularis* at a volcanic CO₂ vent and two nearby reference sites with ambient pH and no vent activity along the coast of Ischia, Italy (Figure 1). The CO₂ vent system is located at a 5 m depth inside a semi-submerged cave of volcanic origin named *Grotta del Mago* (Magician's Cave, 40°42'41.87"N, 13°57'51.06"E, hereafter Vent system) (Figure 1). The cave (total length of 110 m) consists of a main outer chamber (10 m wide x 30 m long), connected to an inner chamber by a long narrow passage (Cinelli et al., 1977). Published studies and personal observations indicated an increase in the CO₂ vent activity over the last 50 years in the main chamber, with limited vent activity in the 70's (Cinelli et al., 1977) and 2000's (Dappiano & Gambi, 2004) developing into intense activity from 2014 onwards. The abundance of *A. calycularis* in the cave has increased over time, with a low and patchy distribution between 1-2 m depth in the main chamber in the 1970's (Cinelli et al., 1977) to a high and continuous distribution in the 2000's (Dappiano & Gambi, 2004). The present study was performed in the main chamber of the cave. The reference sites with ambient pH were chosen following the criteria: i) *A. calycularis* naturally occurred there, ii) they hosted similar habitats and depths as the CO₂ vent site, and iii) and no venting activity was evident. Two reference sites were selected: Punta Vico (40°45'32.28"N, 13°52'55.38"E, another semi-submerged cave, with a main chamber 10 m wide x 30 m long, 5 m maximum depth, hereafter Ambient 1); and Sant'Angelo (40°41'33.78"N, 13°53'38.88"E, an overhang, also a natural habitat of *A. calycularis*, located on a natural arch, with an opening of 10 m wide x 10 m height, 10 m maximum depth, hereafter Ambient 2). Initial investigations of the natural systems and environmental parameters started in June, 2016. These preliminary environmental data were used to plan subsequent field

163 samplings of the carbonate chemistry associated with the CO₂ vent system and reference sites in
164 September, 2018 and June, 2019.

165 **2.2 The coral**

166 *A. calycularis* (Pallas, 1766) is an azooxanthellate scleractinian colonial coral endemic to the
167 Mediterranean, characterized by the bright orange color of its coenosarc and polyps (Zibrowius,
168 1995). It is considered a long-lived species (*e.g* large colonies may have a life span of several
169 decades) and commonly found in dimly lit, shallow rocky habitats (vertical walls, cave entrances,
170 overhangs, from the intertidal fringe to 50 m depths) (Zibrowius, 1995). It can be highly abundant
171 covering more than 90% of local reefs. It has a limited geographic distribution, with a southwestern
172 distribution in the Mediterranean Sea (Zibrowius, 1995). This coral is considered a warm-water
173 species with a narrow temperature tolerance confined to 14°C during the winter (Bianchi, 2007).
174 Fossil records reveal this species lived in the northwestern Mediterranean during part of the
175 Pleistocene, where climatic fluctuations occurred leading to a reduction of the species (Zibrowius,
176 1995). Interestingly, observed records north of its known distribution range in Italy and Croatia
177 suggest that it is currently expanding northward (Bianchi, 2007). Currently, *A. calycularis* is
178 assessed as vulnerable on the IUCN Red List due to its limited geographic distribution and the
179 historical and current regression caused by human activities in the littoral zone. *A. calycularis*
180 broods its larvae and has relatively low dispersal capacity (Casado-Amezúa et al., 2012).

181 **2.3 Gas and temperature**

182 Gas samples were collected in 200 ml glass bottles and analyzed using gas chromatography
183 (Agilent 7890B combined with a Micro GC analyzer-INFICON, held at a constant temperature of
184 80 °C). The mean composition of the bubbling gas was predominantly CO₂ (92-95%, with
185 undetectable levels of sulfur gas <0.0002 %) and did not elevate the temperature (see Supporting

Note 1, Figure S1), subsequently resulting in water acidification. Vent activity was sampled by counting the number of vents in randomly placed 1 m² quadrats (n= 11) in the main chamber, with approximately 5 vents m⁻² (mean \pm SE= 4.9 \pm 2.7 vents m⁻², min= 2 vents m⁻²; maximum = 11 vents m⁻²). Temperature was registered every hour by *in situ* temperature data loggers (Hobo TidbiT v2, Onset) in the cave and the reference areas and followed ambient seasonal fluctuations, from 14.7 to 15.2 °C in winter (n=16,754), and from 25.5 to 26.5 °C in summer (n= 19,011) over a 3-year period from 2016 to 2019 at 2 m depth (Figure S1, Table S1).

2.4 pH_T time series, pH_T variability and pH sensor calibration

SeaFETTM Ocean pH sensors (Satlantic) were deployed to quantify variation in pH inside the cave at 2, 3 and 4 m depth. They were deployed in May-June (before summer) and in September (after summer) to assess whether differences in water temperature stratification could influence pH across depths. Dates of deployment were from September 8 to September 24, 2018 and from May 30 to June 18, 2019. Two sensors were deployed in the reference areas during the same period (Ambient 1 in September, 2018 and Ambient 2 in June, 2019). Before deployment, the SeaFETs were calibrated with ambient pH water in the aquarium facilities at the Center Villa Dohrn (Ischia, Italy) (for full details of pH sensor calibration, see Supporting Methods). The mean offset between calibration samples and calibrated SeaFET pH was \pm 0.002 units, indicating high quality pH dataset (Figure S2).

2.5 Carbonate Chemistry and Nutrients

Discrete water samples were collected using Niskin bottles at the vent and reference areas with ambient pH to measure: i) the carbonate system parameters during the pH sensor deployment, and ii) dissolved inorganic nutrients. Salinity was measured using a CTD (CTD Sea Bird Electronics SBE 19 Plus Seacat). Samples for total alkalinity (A_T) were collected using standard operating

protocols (for full details, see Supporting Methods). The HCl (0.1 M) titrant solution was calibrated against certified reference materials distributed by A.G. Dickson (CRM, Batches #153, #171, and #177). Precision of the A_T measurements of CRMs was $< 2.0 \mu\text{mol kg}^{-1}$ from nominal values. Means were reported as (mean \pm SD): $A_T = 2562.41 \pm 7.8 \mu\text{mol kg}^{-1}$, $n = 27$ in September 2018; and $A_T = 2543.57 \pm 21.78 \mu\text{mol kg}^{-1}$, $n = 21$ in June 2019. A_T and pH_T were used to determine the remaining carbonate system parameters at *in situ* temperature and depth of each sampling period in the R package seacarb v3.2.12 (for constant details, see Supporting Methods). Dissolved inorganic nutrients (nitrite NO_2 , nitrate NO_3 , ammonium NH_4^+ , phosphate PO_4 and silicate Si(OH)_4) were determined using a colorimetric method (Supporting Methods) (Table S2).

2.6 Coral field surveys: cover, population structure and morphology

The *A. calycularis* cover was quantified using 24 photoquadrats (25 x 25 cm) positioned along six transects at four depths: 1, 2, 3, and 4 m in the three study sites (Vent, A1, A2). Percentage cover was analyzed with ImageJ image software (National Institutes of Health, <https://imagej.net/ImageJ>). Size frequency-distribution was calculated at 1 and 3 m depths by counting the number of polyps of each colony and each colony was then pooled into one of five size classes (I: 1-5 polyps; II: 6-10 polyps; III: 11-15 polyps; IV: 16-20 polyps; V: > 20 polyps). These size classes were selected to span the range of colony sizes encountered in the field. We also assessed necrosis as the percentage of the colony exhibiting dead tissue or denuded skeleton, from white-grey to unpigmented or denuded skeleton. Finally, visual assessments were used to classify the colonies into two morphological categories: encrusting (flat growth form) and massive (extensive vertical and lateral growth). Encrusting colonies extended laterally over the surrounding substrate, whereas massive presented a greater vertical accretion which resulted in semi-spherical

shapes. This categorical criterion allowed us to obtain two simple morphological variables to capture biologically relevant axes of variation.

2.7 Sample collection for presence of coenosarc, skeletal characteristics and growth

Sixty-six colonies of *A. calycularis* were sampled haphazardly for coenosarc, biometric, growth, and skeletal parameters. Thirty-four colonies were collected at the vent site: 16 colonies were obtained from the vicinity of the CO₂ vents at 3 m depth (vent system deep, Vd) and 18 colonies at 1- 2m depth (vent system shallow, Vs). Thirty-two colonies were collected from areas with ambient pH conditions: 17 colonies in Punta Vico, Ambient 1, 1 – 2 m depth; and 15 colonies in Sant'Angelo, Ambient 2, 1 -2 m depth. The 66 colonies were photographed and the percentage of coenosarc (*i.e.*, the living tissue connecting the polyps) was determined. The % of coenosarc was determined from the edges of the polyp tissue. The % of coenosarc was classified into ten classes at every 10% interval, from 100% to 0%. Loss of coenosarc in *A. calycularis* may occur mainly by two mechanisms: 1) loss of tissue due to necrosis (when colony exhibits dead tissue, from white-grey to unpigmented or denuded skeleton), or 2) the coenosarc is already absent due to physiological and morphological characteristic of the colonies.

2.7.1 Biometric parameters

Coral skeletons were rinsed in a solution of 10% commercial chlorine bleach for 3-4 days to dissolve polyp tissue, then they were dried at room temperature for 3 days. Colony was defined as the whole calcareous skeleton, which included the polyps (corallites) and the coenosteum. The following parameters were measured: colony length (L_c , major axis of the colony) and colony width (W_c , minor axis of the colony); number of polyps in each colony (NP_c), corallite length (L_p , maximum axis of the oral disc) and corallite width (W_p , minimum axis of the oral disc) (for full details, see Supporting Methods, Figures S3-S4, and Tables S3-S4).

2.7.2 Growth and age estimations

The age of each corallite skeleton was determined by counting the growth bands of 49-70 randomly selected corallites per site, by means of computerized tomography (CT). Growth bands are distinguished by a high-density band in winter and a low-density band in summer in temperate corals (see Supporting Methods). The age of all collected corallites was estimated using the von Bertalanffy's length-age growth function derived from the CT growth bands analysis. Coral growth is described by three parameters: linear extension rate (linear growth), net calcification rate (net mass deposited) and bulk skeletal density (mass per volume unit) (Goffredo et al., 2009). The measurement of all three components is fundamental when assessing the effect of the environment on coral growth, since none of the three parameters is a perfect predictor for the other two and each species can respond differently to environmental conditions. Then, the following three coral growth parameters were calculated for both polyp and colony levels: 1) linear extension rate; 2) net calcification rate and 3) bulk skeletal density (see below for bulk skeletal density measurements) (for full details, see Supporting Methods).

2.7.3 Skeletal parameters

Skeletal parameters of colonies were calculated by applying the buoyant weight technique through the density determination kit of the Ohaus Explorer Pro balance (± 0.0001 g; for further details, see Supporting Methods). This method is based on the Archimedes principle applied to a specimen after full saturation with the same fluid in which it was submerged. The measurements required to calculate the skeletal parameters were: density of the fluid medium (ρ); dry mass (DW), buoyant weight of the skeleton (BW= weight of the skeleton minus weight of the water displaced by it), SW (saturated weight of the coral = weight of the skeleton plus weight of the water enclosed in its). Measurements were repeated three times to get an average for BW and SW. Based on these

measurements, the following parameters were calculated: V_{MATRIX} (matrix volume = volume of the skeleton, excluding the volume of its pores); V_{PORES} (pore volume = volume of the pores in the skeleton), V_{TOT} (bulk volume = total volume of the skeleton including its pores). Finally, the skeletal parameters of colonies were calculated: the micro-density (ratio of DW to V_{MATRIX}); the bulk density (ratio DW to V_{TOT}); and the porosity (ratio V_{PORES} to V_{TOT}).

2.8 Sample collection for genetics and transcriptome assembly

A. calycularis colonies were haphazardly collected between 1- 2 m depth to compare gene flow among populations at the study sites. Nineteen colonies from the Vent, 14 colonies from Ambient 1 and 8 colonies from Ambient 2 were sampled for genetic analysis. RNA was extracted from a single polyp of each colony using a RNeasy kit (Qiagen Inc., Valencia, CA, USA) according to the manufacturer's instructions (for full details, see Supporting Methods). Approximately 1 μg of RNA was used to construct a cDNA library for each sample using the Illumina TruSeq RNA v2 Kit (Illumina, San Diego, CA, USA) (see Supporting Methods).

Libraries were sent to the Genomics Core Facility of the Health Sciences Cores at the University of Utah (Salt Lake City, Utah, USA) and samples were quantified using a Bioanalyzer (Agilent, Santa Clara, CA, USA) (see Supporting Methods). We assembled the first *de novo* transcriptome of *A. calycularis* with samples collected from Ischia. The following programs and scripts were run on Stanford University's Sherlock cluster and all scripts used in this pipeline (https://github.com/bethsheets/Astroides_transcriptomics) along with a general guide are available on GitHub (doi:10.5281/zenodo.2580291). Four population-specific *de novo* assemblies were generated using three individuals per population for each population in the program Trinity-2.8.4 (see Supporting Methods). Prior trials mapping to available corallimorpharian genomes produced incomplete assemblies. Therefore, assembled contigs were validated to be included in the

assembly by filtering for only metazoan matches found in the combined UniProt's Swiss-Prot and TrEMBL databases using BLASTX in the BLAST+ toolkit (see Supporting Methods). Matches were considered significant at values of $\leq 1 \times 10^{-3}$ and the top hit for each contig was kept for assembly filtering and annotation. Transcriptome completeness was assessed using BUSCO v3 (see Supporting Methods) against the metazoan (obd9) set. BUSCO analyses revealed that the final combined transcriptome was 97% complete (949 complete BUSCOs out of 978 searched: 366 complete single-copy, 583 complete and duplicated; 12 fragmented, and 17 missing). For the 41 individuals used for population analyses, the average overall mapping rates for each population were as follows: Vent-Grotta Mago 79% (range 71.91 - 85.28), Ambient 1- Punta Vico 80% (range 65 – 84.74), Ambient 2- Sant' Angelo- 80.26% (range 71.91 - 85.28). After filtering, we detected 46,784 biallelic SNPs among the vent and two ambient populations.

2.8.1 Mapping and SNP detection

For all 41 samples, raw paired- and single-end sequence files were mapped to the *de novo* assembly using HISAT2 (see Supporting Methods) with the very-sensitive setting. Duplicate reads due to PCR were removed with Picard tools (<http://broadinstitute.github.io/picard/>) MarkDuplicates using the lenient validation stringency. Overall mapping rates were compared among populations to assess whether certain populations were preferentially mapping to the *de novo* assembly. Transcriptome-derived single nucleotide polymorphisms (SNPs) were called on all individuals using SAMtools mpileup and BCFtools (for filter settings, see Supporting Methods).

2.8.2 Identifying SNP candidates for environmental selection in high CO₂ conditions and enrichment analysis

We identified potential outlier SNPs related to the CO₂ vent location. We calculated pairwise F_{st} estimates (Vent - Ambient 1, Vent - Ambient 2, Ambient 1 - Ambient 2) per locus using the basic

stats function with HIERFSTAT package in R (see Statistical analyses). We used these estimates to compare the genetic distance for each SNP between the three populations $[F_{ST}(\text{Vent-A1}) + F_{ST}(\text{Vent-A2})]/F_{ST}(\text{A1-A2})]$. To identify potential outlier SNPs related to the CO₂ vent location, we compared the genetic distance for each SNP for the population comparisons including Grotta Mago to the genetic distance between the ambient populations A1 and A2 $[F_{ST}(\text{Vent-A1}) + F_{ST}(\text{Vent-A2})]/F_{ST}(\text{A1-A2})]$. SNPs with values over 2 showed an excess of genetic differentiation in the CO₂ Vent compared to the other ambient pH populations. Using the transcriptome assembly annotations, we searched for enrichment patterns in the contigs holding these candidate SNPs by using their UniProt identifiers (<https://www.uniprot.org/>) in a Gene Ontology (GO) search (<http://geneontology.org/>).

2.9 Statistical analyses and data visualization

Environmental data analyses: Temperature, pH_T, SeaFET sensor calibration, carbonate chemistry and figures were performed using the R packages: seacarb v3.2.12 and ggplot2 v3.1.1 (see Supporting Methods for R package references). Carbonate system parameter figures in the vent system were created with Ocean Data View software (version 5.1.2, <http://odv.awi.de>). *Biological surveys:* A linear mixed model was used to test for differences in % cover (logit transformation) as a function of site (fixed factor, 3 levels), depth (fixed factor, 4 levels) and quadrat as a random

effect. Chi-square contingency tables were used to compare the size–frequency distributions among sites, as well as the frequency of encrusting and massive forms. Kolmogorov-Smirnov two-sample tests were used to determine whether there were significant differences in necrosis between the CO₂ vent and ambient pH sites. These analyses were computed using lme4 v1.1.21 package implemented in R. *Skeletal characteristics and growth*: Relationships between biometrical and skeletal parameters were calculated using the power function model. Pearson’s correlation coefficients were calculated for the relationships among biometric and skeletal parameters at both colony and polyp levels. Spearman’s rank correlation coefficient was used to calculate the significance of the correlations between colony biometric and skeletal parameters and pH_T. ANOVA was used to test % cenosarc (with arcsin transformation), mean mass, polyp number, bulk density, linear extension rate, calcification rate, and porosity of the colonies and mean length of corallites among sites. We used the non-parametric Kruskal-Wallis test for differences in means for data that did not meet the assumption for normality and equal variance. Kruskal-Wallis tests were applied to mean area, length, width, micro-density of colonies, corallite mean age, polyp linear extension rate, net calcification rate, and length of central and all corallites. These analyses were computed using IBM SPSS Statistics 12.0 (IBM Corporation). The Von Bertalanffy growth model and confidence intervals (CI) were estimated through a regression analysis by least squares procedure using raw data of corallite length and age (measured by computerized tomography) (see Supporting Methods). These analyses were carried out in the software MATLAB R2012a (MathWorks, Natick, USA). *Population genetics*: Population genetic analyses of SNPs, Weir and Cockerham’s pairwise F_{ST} estimates among populations, and the heatmap of divergent SNP genotypes were conducted in the R-based program HIERFSTAT v4.22 and ComplexHeatmap v2.4.2, respectively.

3. RESULTS

3.1 Carbonate Chemistry Associated with the CO₂ vent system in the *Grotta del Mago* cave

The CO₂ vent system occurs at a 5 m depth inside the main chamber of the cave *Grotta del Mago* with approximately 5 vents m⁻² (Figure 1) and do not elevate temperature (Table 1, Figure S1, Table S1). The carbonate chemistry derived from discrete water samples and *in situ* monitoring of seawater pH_T (pH on the total scale) delineated a pH_T gradient from 4 m to 2 m depth caused by the distance from the bubbling of CO₂ gas from the seafloor (92-95% CO₂, with undetectable levels of sulfur gas < 0.0002 %, see Supporting Note 1) (Figure 1, Table 1). pH sensors revealed reductions in mean pH_T at each depth associated with increased temporal variability in pH_T (Figure 1, Table 1, Figure S5, Table S5). Mean pH_T were: 7.65 to 7.88 at 2 m; 7.62 to 7.74 at 3 m, and 7.60 to 7.60 at 4 m, respectively (see Table 1 and Table S5 for detailed pH statistics). At 2 m depth, 14% and 56% of the pH_T measurements were below 7.8 (projected average global sea surface pH value for the year 2100 with the high emission scenarios RCP8.5) (Gattuso et al., 2015) in June and September, respectively (Table S5). The percentage rose to 34% and 61% at 3 m depth, and 55% and 66% at 4 m depth, in June and September, respectively (Table S5). This pattern of depth-dependent low pH_T was also manifested as extreme pH events (defined as the pH value of 0.4 units less than the mean pH for each depth) that increased in number and duration with depth (Table S6). Mean pH_T and variability were influenced by temperature stratification in June and September (Figure 1, Figures S5-S6). This is because during periods of stratification, and hence reduced vertical mixing (Turner, 1973), the input of CO₂ is likely to be primarily confined to the lower part of the water column, leading to lower pH values near bed than when the water column is well mixed. The mean temperature difference between 2 m and 4 m in June was 0.25 °C, whereas the mean temperature difference was only 0.02 °C in September (Figure S6). In September, reductions

in seawater pH_T were driven by increased dissolved inorganic carbon concentrations (C_T) and higher pCO_2 concentrations at relatively constant total alkalinities (A_T) and temperatures across depths (Table 1, Figure S5). Mean pCO_2 ranged from $2905 \pm 1664 \mu\text{atm}$ at 2 m, to $3146 \pm 1928 \mu\text{atm}$ at 3 m, to $3192 \pm 1806 \mu\text{atm}$ at 4m depth, and aragonite saturation state (Ω_a) ranged from 1.10 ± 0.4 at 2m, to 1.05 ± 0.4 at 3 m, and to 1.02 ± 0.4 at 4m depth (Table 1). In contrast, in June, the vent site was characterized by an increase in temperature along the water column (from $\sim 18.5^\circ\text{C}$ to $\sim 25^\circ\text{C}$), which created greater difference across the three depths in terms of pH_T and associated carbonate chemistry parameters, particularly for the pCO_2 concentrations (from $1531 \pm 627 \mu\text{atm}$ at 2 m, to $2082 \pm 1502 \mu\text{atm}$ at 3 m, and $2812 \pm 2310 \mu\text{atm}$ at 4 m depth) and Ω_a (from 1.44 ± 0.27 at 2 m, to 1.23 ± 0.35 at 3 m, to 1.05 ± 0.42 at 4 m depth) (Table 1, Figure S5). At the two ambient pH sites, the mean pH_T ranged from 7.97 to 8.05 units, pCO_2 from 322 ± 34 to $586 \pm 76 \mu\text{atm}$, and Ω_a from 3.54 ± 0.23 to 3.86 ± 0.23 (Table 1).

3.2 Cover, population structure, and morphology of *A. calycularis*

The CO_2 vent population was characterized by small colonies (90% colonies had up to 10 polyps) and no large colonies of more than 20 polyps (class V) with massive morphology were found (Figure 2, Figure S7). Larger colonies (*i.e.* > 16 polyps, size classes IV and V) were only found in the two reference areas (percentage of larger size classes ranged from 13% in A1 to 16 % in A2), which differed significantly among the CO_2 vent site ($\chi^2 = 91.9$, $df = 8$, $p < 0.0001$). Additionally, necrosis was significantly higher at the CO_2 vent site ($13 \pm 4\%$) than the reference areas (both $< 0.5\%$, $D = 0.56$, $p < 0.0001$). *A. calycularis*' cover at the CO_2 vent site decreased from 50% at 1 m depth, to 30% at 2m, 9% at 3 m, and 1% at 4m depth, as seawater pH_T also declined (Figure S7). This decline in coral cover was also observed in Ambient 1 (also a cave, from 69% at 1 m to 14%

at 3 m) but not in Ambient 2 (overhang, from 72% at 1 m to 62% at 3 m; $F = 14.1$, $df = 11, 55$; $p < 0.001$) (Figure S7).

3.3 Coenosarc, skeletal parameters and growth

Percentage of coenosarc (the living tissue connecting the polyps) significantly decreased between ambient pH sites (87 and 70%) and the CO₂ vent (28 and 14%) (Figure 2, $p < 0.0001$). Mean colony area decreased by ~ 80 - 71% and mean polyp number by ~ 27 - 18% at the Vent deep compared to ambient pH sites ($p < 0.001$) (Figure 3A). The skeletal parameters that characterize the architecture of colonies showed different patterns in relation to pH (Figure 3A-B, Figures S8-S9). Bulk density (ratio dry mass to bulk volume) and micro-density (ratio of dry mass to matrix volume) increased at low pH, while porosity (ratio pore volume to bulk volume; see Methods) decreased at low pH ($p < 0.001$; Figure 3A-B). Colonies at the CO₂ vent deep presented higher bulk density (~ + 27 %) and micro-density (~ + 7 %) and lower porosity (~ -28 %) compared to colonies from the ambient pH sites ($p < 0.001$) (Figure 3A-B, Figure S9).

Growth parameters of *A. calycularis* differed significantly between the CO₂ vent site and ambient pH sites (Figure 3B, Figure 4, Figure S10, Table S7). Mean polyp growth rate decreased exponentially with age at all sites (Figure S10). Young individuals (1–3 years old) grew relatively rapidly ($> 2 \text{ mm yr}^{-1}$), but, as they aged, their skeletal growth rate decreased ($< 1.3 \text{ mm yr}^{-1}$ at 8–10 years old) (Figure 4, Tables S7-S8). A trend toward higher linear extension and net calcification rate was observed at low pH at the polyp level (Figure 3B, Table S7). Polyp net calcification rate ranged from $3.95 \text{ mg mm}^{-2} \text{ yr}^{-1}$ at Vent deep, to $3.04 \text{ mg mm}^{-2} \text{ yr}^{-1}$ at Vent shallow, to $2.39 \text{ mg mm}^{-2} \text{ yr}^{-1}$ and $2.06 \text{ mg mm}^{-2} \text{ yr}^{-1}$ at ambient pH sites (Table S7). This indicates that net calcification rates increased approximately by 48%-93% from the more acidified (Vent deep) to the less acidified (Vent shallow) to the non-acidified (ambient pH) locations at polyp level. Linear

extension and net calcification rates at colony level were homogenous in ambient pH and acidified conditions (Figure 3B, Table S7).

3.4 Transcriptome assembly and population genomics

The *A. calycularis* transcriptome composed of 12 colonies contained 113,351 contigs with an N50 of 2,285 (range 501 – 38,179). Based on 46,784 SNPs in 41 individuals, PCA analysis revealed strong clustering by population (Figure 5). The vent population in Grotta Mago was most distinct along PCA axis 1, but overlapped with Ambient1 (PV) along axis 2. Pairwise F_{ST} measurements also support strong population structure within each of the three locations: CO₂ vent (Grotta Mago) – Ambient 1 (Punta Vico) = 0.034, CO₂ vent (Grotta Mago) – Ambient 2 (Sant'Angelo) = 0.026, Ambient 1 (Punta Vico) – Ambient 2 (Sant'Angelo) = 0.024. SNPs with values over 2 show an excess of genetic differentiation in GM compared to the other populations. There were 334 loci with an excess F_{ST} ratio of 10 or more, out of 2246 loci in our data set with known molecular function. An analysis of the 402 unique molecular function Gene Ontology (GO) terms associated with these loci showed there to be three significant enrichment classes (Table S9): calcium ion binding (12 loci, $p_{adj} = 7 \times 10^{-23}$), catalytic activity (4 loci, $p_{adj} = 2 \times 10^{-9}$), and oxidoreductase action (12 loci, $p_{adj} = 0.05$).

Calcium ion loci include calmodulin, calcineurin, calnexin, calcium-binding proteins in the sarcoplasmic reticulum, and a set of two poorly characterized proteins with calcium binding motifs (Contigs 3436 and 7780). These proteins are EF-hand calcium-binding protein and C-type lectin calcium-binding in a hmmer database search (<https://www.ebi.ac.uk/Tools/hmmer/>). Because

calcium ion control is particularly central to calcification in scleractinians, we examined the 77 SNPs from the thirteen calcium-related loci for patterns across populations (Figure 6). As expected, the Grotta Mago population had highly divergent SNP genotypes at these loci (average minor allele frequency difference of 0.24), but these genes also showed a strong degree of linkage among SNP genotypes within a single gene often across 1000s of base pairs (Figure 6). Such multi-SNP haplotypes are rare in our data set yet occur in 8 of 10 high excess, calcium ion loci with multiple SNPs.

Given the strong differences in calcium management suggested by excess differentiation of calcium ion genes in Grotta Mago, we queried our transcriptome SNP data base for other genes potentially involved in calcification. In corals, calcification occurs in the calicoblastic space through a combination of high calcium concentration and high pH (reviewed in Drake et al., 2020). High pH is achieved through proton transport by specific calcium/proton pumps, including the plasma membrane calcium ATPase (PMCA). There were no PMCA polymorphisms in our data set, but the V-type ATPase proton pump (contig DN1551, SNPs 1701-1805) showed six of seven SNPs with strong differentiation in Grotta Mago (excess 0.03 -28.8, average 11.4, Figure 6). Minor allele frequencies differed by about a factor of 2 in Grotta Mago compared to the other locations, and SNPs show strong linkage.

In addition to genes involved in calcium and pH regulation, we explored possible adaptation in genes managing intracellular carbonate chemistry. Coral calcification depends on the delivery of CO₂ to the calicoblastic layer where it is converted to carbonate ions (Cohen & McConnaughey,

2003). In *A. calycularis*, a plethora of carbonate related genes showed high differentiation and high linkage in Grotta Mago, including carboxylases and transporters, but the most interesting is a carbonic anhydrase (Contig 15508, 5 of 12 SNPs with excess F_{st} above 10, average=10.3). Carbonic anhydrases convert highly diffusive CO_2 into charged carbonate ions, localizing them in the calicoblastic layer and regulating calcification (Chen, Gagnon, & Adkins, 2018), though they also play a role in pH regulation of non-calcifying coral cells (Bertucci et al., 2013).

4. DISCUSSION

This study contributes to increasing our understanding of how coral populations persist under naturally high pCO_2 environments – and therefore how they might cope under future ocean acidification scenarios – and links trait-shifts with local variation in environmental parameters found in this new CO_2 vent system. Our results expand upon previous research on populations of corals exposed to naturally elevated pCO_2 (Crook, Cohen, Rebolledo-Vieyra, Hernandez, & Paytan, 2013; Enochs et al., 2015; Fabricius et al., 2011; Fantazzini et al., 2015), demonstrating unexpected shifts in patterns of skeleton and growth of the azooxanthellate coral *A. calycularis*. Specifically, colonies shift to a skeletal phenotype characterized by encrusting morphology, smaller size, reduced coenosarc tissue, fewer polyps, and less porous and denser skeletons at low pH. However, while individual polyps calcified more (greater net calcification rates), calcification rate of whole colonies were similar across sites. The resulting colony skeletons showed equal linear extension at low and ambient pH conditions, while their polyp skeletons extended faster in acidified conditions (Figure 7). Transcriptomic data revealed strong genetic differentiation among local populations of this low-dispersal species. We found excess differentiation in the Grotta Mago population for genes central to calcification, including genes for calcium management

(calmodulin, calcium-binding proteins), pH regulation (V-type proton ATPase), and carbonate localization (carbonic anhydrase).

Environmental variability in the CO₂ vent system

The vent system exhibits high temporal variability in seawater pH due to varying CO₂ venting intensity from the seabed, mixing due to variations in stratification, and fundamental thermodynamics processes fundamental to the carbonate system (Takeshita et al., 2015). The carbonate chemistry and *in situ* monitoring of seawater pH delineated a pH gradient (from 4 to 2 m depth) caused by the distance from the venting. This acidification gradient is important for the colonies exposed to more (deep) or less (shallow) acidified conditions, as reflected by the biological response of *Astroides*. The conditions in these zones are comparable with IPCC projections for near future acidification scenarios (RCP2.6 and RCP8.5), which project a decrease in surface pH from -0.14 to -0.4 pH units by 2100 relative to 1870 (Gattuso et al., 2015). pH and its variability found in this study are comparable with the range of natural variation observed in other CO₂ vent systems, with fluctuations of 0.6, 0.7 and 0.5 pH units in coral reefs (Agostini et al., 2018), temperate reefs in Panarea (Prada et al., 2017) and in other CO₂ vents in Ischia (Teixidó et al., 2018), respectively. Likewise, Hofmann et al. (2011) reported pH fluctuations between 0.024 to 1.430 pH units, in which pH measurements were taken from different locations, ranging from polar to tropical, and open-ocean to coastal areas. Interestingly, as mean pH was reduced, its variability and the percentage of pH_T measurements registered below 7.8 units increased, when seawater was uniformly warm. In contrast, in June when the water column was stratified, pH and its variability near the bottom was similar to what was observed in September whereas, farther

from the bottom, pH was higher and less variable. These results indicate that seawater stratification may play a key role in controlling the temporal and depth patterns of pH/pCO₂.

Shifts in coral skeleton, growth, and coenosarc

Each scleractinian coral species may adopt different growth strategies in response to ocean acidification. For example, investing calcification resources in bulk skeletal density by sacrificing the rate of linear extension has been observed in *Orbicella annularis* (Carricart-Gavinet, 2007). In contrast, investing calcification resources in linear extension rate at the expense of bulk density has been reported for some *Porites* (Lough & Barnes, 2000) and Dendrophyllidae species (Goffredo et al., 2009). Both strategies may imply different ecological trade-offs for the coral: investing in a denser skeleton results in greater resistance to mechanical stress, while increasing linear extension rate may be advantageous for space competition and earlier sexual maturity (Goffredo et al., 2009). Unexpectedly, *A. calycularis* revealed unusual patterns in the calcification response to ocean acidification, such as higher bulk skeletal density and lower porosity while maintaining colony linear extension rates and net calcification. This response is different to what was previously shown in solitary corals (e.g. *Balanophyllia europaea*) growing in natural low pH conditions, where a decrease of net calcification resulted from preserving linear extension (to reach the polyp size of sexual maturity) at the expenses of lower bulk density (e.g. increased in skeletal porosity resulting in more fragile skeletons) (Fantazzini et al., 2015). Tambutté et al.(2015) found the same response of decreasing calcification and bulk skeletal density while linear extension of skeleton remained unchanged in the tropical coral *Stylophora pistillata* subjected to low pH conditions in laboratory. Mollica et al. (2018) modelled the skeletal growth to changes in seawater chemistry and predicted declines in *Porites* skeletal density but no linear extension across global

reefs, reflecting the large variability in the response of coral calcification to ocean acidification. The authors suggested that under low-pH conditions, the increase in linear extension reflects the elongation of calcium carbonate crystals at the site of calcification, while the increase in skeletal density reflects the lateral thickening of calcified elements of coral skeleton (Mollica et al., 2018). The unusual response of *A. calycularis* to acidification may reflect an overall maintenance of energetic resources allocated to calcification at the level of the colonies, which extended at the same rate but were composed by fewer polyps, thus partitioning the available energy for calcification among fewer polyps (Swain et al., 2018). We can therefore reasonably assume that nutrients levels, and potentially the zooplankton, did not differ among study sites (Supporting Material Table S2). As a result, a single polyp would have more energetic resources available for calcification than in ambient pH conditions, as indicated by their greater skeletal growth parameters. This particular response may be possible in *A. calycularis* due to its colonial nature. We hypothesize that in order to maintain the calcification rate at the colony level, colonies tend to decrease their number of polyps, but in turn, their few polyps extend their skeleton faster to reach the size of sexual maturity. No asexual division (fragmentation) has been observed over 5 years in *A. calycularis* in the three study sites, suggesting that this strategy of reproduction is not common. *A. calycularis* exhibited at the vent site a morphological shift to encrusting and smaller colonies, with less porous, and potentially more robust corallite skeletal architecture. While individuals from the vents were composed of corallites with higher skeletal density, this was less evident at the colony level. While skeletal integrity was not strictly quantified, observations at the vent site showed that the colonies were more fragile and lost their integrity more readily, suggesting that the section of the skeleton located between the polyps (coenosteum) was either less calcified and/or more prone to dissolution. This could be the result of thinner or

absent coenosarc (the tissue covering the coenosteum) found in the colonies at the CO₂ vent. Contrasting responses between skeletal parts that either are or are not protected by living tissues has already been reported for corals (Hennige et al., 2015; Ries, 2011; Rodolfo-Metalpa et al., 2011). This loss of coenosarc could indicate the beginning of a further shift from colonial forms towards solitary polyps to ensure survivorship, as has occurred throughout the history of scleractinian coral evolution and in laboratory conditions (Fine & Tchernov, 2007; Kvitt et al., 2015). Interestingly, it was recently shown that following a heatwave and a bleaching event, the Mediterranean coral *Cladocora caespitosa* suffered from apparent mortality but its tissues actually retracted inside the individual corallites before rejuvenescence occurred a few years later (Kersting & Linares, 2019). Here, we hypothesize that a similar, but less extreme phenomenon occurred with the corals reducing their coenosarc in response to low pH. A reduction in tissue thickness can have implications for calcification because the precipitation of calcium carbonate occurs in the calcifying fluid that is a medium semi-isolated from the external seawater by the overlying coral tissues. To promote calcification, corals have the ability to upregulate pH and C_T (dissolved inorganic carbon) concentrations in the calcifying fluid (Comeau, Cornwall, & McCulloch, 2017), a capacity that is reduced under ocean acidification (McCulloch, Falter, Trotter, & Montagna, 2012). Here reduced calcification between the polyps was likely due to a reduction of coral ability to maintain optimal carbonate chemistry conditions in the calcifying fluid between the polyps. This could have been the result of natural spatial heterogeneity sensitivity of colonies to acidification (Holcomb et al., 2014). In addition to reduced calcification, thinning or disappearing of the tissues likely led to local dissolution because exposed skeletons are more prone to dissolution (Ries, 2011). As a result of reduced calcification and dissolution of the coenosteum, colonies at the vent site were weaker and smaller despite heavily calcified corallites.

585

586 *Genomics of differentiation of corals at the CO₂ vent system*

587 Our results show strong genetic differentiation of all three *A. calycularis* populations (F_{ST}
588 averaging 0.024 – 0.034), with over 5000 SNPs showing $F_{ST}>0.10$. A previous genetic study of *A.*
589 *calycularis* using microsatellites also found significant genetic differentiation at km-scale
590 distances, likely a reflection of this species limited dispersal capabilities (Casado-Amezúa et al.,
591 2012). These data showed strong linkage among SNPs across 1000s of bp within genes and strong
592 linkage across different genes. These patterns could be generated by selective sweeps acting on a
593 small number of founder colonies, but because linkage among genes and SNPs occurs among
594 ambient pH (Ambient 1 and Ambient 2) individuals as well as Vent corals. These linkages were
595 probably not due to recent selection at the CO₂ vent site alone but reflect the underlying
596 architecture of adaptation. *A. calycularis* is a warm-water coral whose distribution range is
597 currently expanding northward (Bianchi, 2007), where Ischia belongs to the north-east margin of
598 the confirmed distribution. As a result, it is also likely that selection is acting at the Ambient 1 and
599 2 sites compared to more southerly populations. Disentangling the ways in which selection at high
600 CO₂ locations combines with selection at higher temperatures may be particularly important in
601 future ocean conditions. The matrix of genetically distinct populations of *A. calycularis*
602 experiencing a variety of selection regimes for heat and CO₂ may be a powerful setting for this
603 future work.

604 The most highly differentiated genes in the vent site population, Grotta Mago, are
605 annotated for calcium regulation, proton pumping, and inorganic carbon regulation. It is
606 possible that they are differentiated in Grotta Mago for reasons other than selection on

607 calcification in the presence of high CO₂. However, the strong shift in alleles at these loci
608 and the linkage among those differentiated SNPs provides a strong set of hypotheses for
609 the way selection might act to favor coral calcification at low pH.

610 Two loci of calmodulin were highly differentiated in Grotta Mago, with linked SNPs in our
611 data set. Calcium transporter genes are thought to be important in delivering calcium to
612 the calicoblastic space (Allemand, Tambutté, Zoccola, & Tambutté, 2011). Though the
613 precise mechanism is not known, calmodulin along with calbindin and calreticulin are
614 hypothesized to play a role in managing calcium levels and can be sensitive to pH
615 (Allemand et al., 2011). For example, Kaniewska et al. (2012) showed 8-fold down
616 regulation of calmodulin in a CO₂-treated reef building coral. An increase in calcium at the
617 site of calcification has been shown as a mean to alleviate the negative effect of low pH in some
618 corals (Decarlo, Comeau, Cornwall, & McCulloch, 2018). Our data also showed excess
619 differentiation in genes that depend on calcium concentrations for their function, such as
620 calineurin, calnexin and the sarcoplasmic reticulum histidine-rich calcium-binding protein,
621 which are thought to play a role in calcium homeostasis.

622 Intracellular and vacuolar H⁺ concentrations are central to coral calcification by controlling
623 pH of the calcifying fluid and the calicoblastic and gastrodermal cells. The V-type ATPase
624 proton pump is localized in the symbiosomes of corals that contain intracellular symbionts
625 (Tresguerres, 2016), but is also highly expressed in non-symbiotic gastroderm of
626 symbiont-free tips of quickly calcifying corals, suggesting a role in calcification in the
627 absence of symbionts (Perez, 2015). In particular, the protein VHA (V-type proton
628 ATPase) is differentially regulated in corals exposed to low pH, being downregulated
629 more than four fold in experiments on the reef building coral *Acropora millepora*
630 (Kaniewska et al., 2012). The population of *A. calicularis* in Grotta Mago showed strong
631 differentiation at 6 SNPs across a 100 bp region of this gene.

632 CO₂ diffuses very quickly through cells, and is hard to localize in cell regions that need it
633 for photosynthesis or calcification. Carbonic anhydrase catalyzes the reaction to convert
634 CO₂ to carbonate ions that diffuse much less quickly. As a consequence, carbonic
635 anhydrase is central to calcification in many marine species. In fact, Zebral et al. (2019)
636 suggest use of it as a biomarker to monitor effects of acidification. In corals, carbonic
637 anhydrase is thought to favor carbonate ion concentration in the calicoblastic space and

in symbiosomes through conversion of CO₂ (Chen et al., 2018; Zoccola et al., 2016).

However, low-pH experiments on a deep water coral (*Lophelia pertusa*) did not find strong

shifts in carbonic anhydrase activity, nor did an examination of carbonic anhydrase in

polychaete worms from the Ischia CO₂ vents (Del Pasqua, Gambi, Caricato, Lionetto, &

Giangrande, 2019). Experiments on reef building corals have shown mixed results

(Kurihara, Takahashi, Reyes-Bermudez, & Hidaka, 2018). We found strong differentiation

of one carbonic anhydrase locus in Grotta Mago. An average shift in minor allele

frequency from 0.14 to 0.50 in six linked SNPs may signal differential activity of this gene

in some functionally important way. These SNPs appear to be downstream of the

carbonic anhydrase coding region and if they play a role it may be as allele-specific

regulators of expression. These allele differences may be a good tool to understand the

role of carbonic anhydrase in reaction to high CO₂.

In conclusion, our study demonstrates that the natural population of the azooxanthellate coral *A.*

calycularis living near the CO₂ vent system shows variable responses in terms of skeleton and

growth patterns that result in a shift in phenotypic and ecological traits. We have shown that these

variable responses at the polyp and colony level allow this coral to cope with low and variable pH

in the long term by re-allocating energy investments between individual and colony growth as well

as mineralogical characteristics. Transcriptomic data revealed strong genetic differentiation among local populations with several candidate loci and linkage blocks under selection. In addition, we found excess differentiation in the CO₂ vent population for genes central to calcification, including genes for calcium management (calmodulin, calcium-binding proteins), pH regulation (V-type proton ATPase), and inorganic carbon regulation (carbonic anhydrase). These patterns highlight both the CO₂ vents as well as the fringes of this species' expansion as potential drivers of adaptation.

For Review Only

REFERENCES

- Agostini, S., Harvey, B. P., Wada, S., Kon, K., Milazzo, M., Inaba, K., & Hall-Spencer, J. M. (2018). Ocean acidification drives community shifts towards simplified non-calcified habitats in a subtropical – temperate transition zone. *Scientific Reports*, 8, 11354. <https://doi.org/10.1038/s41598-018-29251-7>
- Allemand, D., Tambutté, É., Zoccola, D., & Tambutté, S. (2011). Coral calcification, cells to reefs. In Z. Dubinsky & N. Stambler (Eds.), *Coral Reefs: An Ecosystem in Transition* (pp. 1–552). Springer. <https://doi.org/10.1007/978-94-007-0114-4>
- Bennett, S., Duarte, C. M., Marba, N., & Wernberg, T. (2019). Integrating within-species variation in thermal physiology into climate change ecology. *Philosophical Transactions of the Royal Society B*, 374, 20180550.
- Bertucci, A., Moya, A., Tambutté, S., Allemand, D., Supuran, C. T., & Zoccola, D. (2013). Carbonic anhydrases in anthozoan corals - A review. *Bioorganic and Medicinal Chemistry*, 21(6), 1437–1450. <https://doi.org/10.1016/j.bmc.2012.10.024>
- Bianchi, C. N. (2007). Biodiversity issues for the forthcoming tropical Mediterranean Sea. *Hydrobiologia*, 580, 7–21. <https://doi.org/10.1007/s10750-006-0469-5>
- Bozinovic, F., Calosi, P., & Spicer, J. I. (2011). Physiological correlates of geographic range in animals. *Annual Review of Ecology, Evolution, and Systematics*, 42, 155–179. <https://doi.org/10.1146/annurev-ecolsys-102710-145055>
- Brandl, S. J., Rasher, D. B., Côté, I. M., Casey, J. M., Darling, E. S., Lefcheck, J. S., & Duffy, J. E. (2019). Coral reef ecosystem functioning: eight core processes and the role of biodiversity. *Frontiers in Ecology and the Environment*, 17, 445–454. <https://doi.org/10.1002/fee.2088>

- 685 Camp, E. F., Schoepf, V., Mumby, P. J., Hardtke, L. A., Rodolfo-Metalpa, R., Smith, D. J., &
686 Suggett, D. J. (2018). The future of coral reefs subject to rapid climate change: lessons from
687 natural extreme environments. *Frontiers in Marine Science*, 5, 4.
688 <https://doi.org/10.3389/fmars.2018.00004>
- 689 Carricart-Gavinet, J. P. (2007). Annual density banding in massive coral skeletons: result of
690 growth strategies to inhabit reefs with high microborers' activity? *Marine Biology*, 153, 1–5.
- 691 Casado-Amezúa, P., Goffredo, S., Templado, J., & Machordom, A. (2012). Genetic assessment
692 of population structure and connectivity in the threatened Mediterranean coral *Astroides*
693 *calycularis* (Scleractinia, Dendrophylliidae) at different spatial scales. *Molecular Ecology*, 21,
694 3671–3685. <https://doi.org/10.1111/j.1365-294X.2012.05655.x>
- 695 Chan, N. C. S., & Connolly, S. R. (2013). Sensitivity of coral calcification to ocean acidification:
696 a meta-analysis. *Global Change Biology*, 19(1), 282–290.
697 <https://doi.org/doi:10.1111/gcb.12011>
- 698 Chen, S., Gagnon, A. C., & Adkins, J. F. (2018). Carbonic anhydrase, coral calcification and a
699 new model of stable isotope vital effects. *Geochimica et Cosmochimica Acta*, 236, 179–197.
700 <https://doi.org/10.1016/j.gca.2018.02.032>
- 701 Cinelli, F., Fresi, E., Mazzella, L., Pansini, M., Pronzato, R., & Svoboda, A. (1977). Distribution
702 of benthic phyto- and zoocoenoses along a light gradient in a superficial marine cave. In B. F.
703 Keegan, P. O. O'Ceidig, & P. J. Boaden (Eds.), *Biology of Benthic organisms* (pp. 173–183).
704 Pergamon Press, Oxford.
- 705 Cohen, A. L., & McConnaughey, T. A. (2003). Geochemical Perspectives on Coral
706 Mineralization. In P. M. Dove, S. Weiner, & J. J. DeYoreo (Eds.), *Biom mineralization* (Vol. 54,

- 707 pp. 151–187). The Mineralogical Society of America, Washington, DC.
- 708 <https://doi.org/10.2113/0540151>
- 709 Comeau, S., Cornwall, C. E., & McCulloch, M. T. (2017). Decoupling between the response of
- 710 coral calcifying fluid pH and calcification to ocean acidification. *Scientific Reports*, 7, 7573.
- 711 <https://doi.org/10.1038/s41598-017-08003-z>
- 712 Crook, E. D., Cohen, A. L., Rebolledo-Vieyra, M., Hernandez, L., & Paytan, A. (2013). Reduced
- 713 calcification and lack of acclimatization by coral colonies growing in areas of persistent natural
- 714 acidification. *Proceedings of the National Academy of Sciences of the United States of*
- 715 *America*, 110(27), 11044–11049. <https://doi.org/10.1073/pnas.1301589110>
- 716 Dappiano, M., & Gambi, M. C. (2004). New data on occurrence of thermophile Scleractinia
- 717 (Cnidaria, Anthozoa) in the Phlaegrean Island (Ischia, Procida, Vivara, Gulf of Naples), with
- 718 special attention to *Astroides calycularis*. *Biogeographia – The Journal of Integrative*
- 719 *Biogeography*, 25, 1–15. <https://doi.org/10.21426/B6110042>
- 720 Darling, E. S., Alvarez-Filip, L., Oliver, T. A., McClanahan, T. R., & Côté, I. M. (2012).
- 721 Evaluating life-history strategies of reef corals from species traits. *Ecology Letters*, 15(12),
- 722 1378–1386. <https://doi.org/10.1111/j.1461-0248.2012.01861.x>
- 723 Decarlo, T. M., Comeau, S., Cornwall, C. E., & McCulloch, M. T. (2018). Coral resistance to
- 724 ocean acidification linked to increased calcium at the site of calcification. *Proceedings of the*
- 725 *Royal Society B: Biological Sciences*, 285(1878), 20180564.
- 726 <https://doi.org/10.1098/rspb.2018.0564>
- 727 Del Pasqua, M., Gambi, M. C., Caricato, R., Lionetto, M. G., & Giangrande, A. (2019). Effects
- 728 of short-term and long-term exposure to ocean acidification on carbonic anhydrase activity and

- 729 morphometric characteristics in the invasive polychaete *Branchiomma boholense* (Annelida:
730 Sabellidae): A case-study from a CO₂ vent system. *Marine Environmental Research*, 144, 203–
731 212. <https://doi.org/10.1016/j.marenvres.2019.01.011>
- 732 Doney, S. C., Fabry, V. J., Feely, R. A., & Kleypas, J. A. (2009). Ocean Acidification: The Other
733 CO₂ Problem. *Annual Review of Marine Science*, 1(1), 169–192.
734 <https://doi.org/10.1146/annurev.marine.010908.163834>
- 735 Drake, J. L., Mass, T., Stolarski, J., Von Euw, S., van de Schootbrugge, B., & Falkowski, P. G.
736 (2020). How corals made rocks through the ages. *Global Change Biology*, 26(1), 31–53.
737 <https://doi.org/10.1111/gcb.14912>
- 738 Enochs, I. C., Manzello, D. P., Donham, E. M., Kolodziej, G., Okano, R., Johnston, L., ... Price,
739 N. N. (2015). Shift from coral to macroalgae dominance on a volcanically acidified reef.
740 *Nature Climate Change*, 5, 1083–1088. <https://doi.org/10.1038/nclimate2758>
- 741 Fabricius, K. E., Langdon, C., Uthicke, S., Humphrey, C., Noonan, S., De 'ath, G., ... Lough, J.
742 M. (2011). Losers and winners in coral reefs acclimatized to elevated carbon dioxide
743 concentrations. *Nature Climate Change*, 1(6), 165–169.
744 <https://doi.org/10.1038/NCLIMATE1122>
- 745 Fantazzini, P., Mengoli, S., Pasquini, L., Bortolotti, V., Brizi, L., Mariani, M., ... Goffredo, S.
746 (2015). Gains and losses of coral skeletal porosity changes with ocean acidification
747 acclimation. *Nature Communications*, 6, 7785. <https://doi.org/10.1038/ncomms8785>
- 748 Fine, M., & Tchernov, D. (2007). Scleractinian coral species survive and recover from
749 decalcification. *Science*, 315(5820), 1811. <https://doi.org/10.1126/science.1137094>

- 750 Gattuso, J.-P., Magnan, A., Bille, R., Cheung, W. W. L., Howes, E. L., Joos, F., ... Turley, C.
751 (2015). Contrasting futures for ocean and society from different anthropogenic CO₂ emissions
752 scenarios. *Science*, 349, aac4722. <https://doi.org/10.1126/science.aac4722>
- 753 Goffredo, S., Caroselli, E., Mattioli, G., Pignotti, E., Dubinsky, Z., & Zaccanti, F. (2009).
754 Inferred level of calcification decreases along an increasing temperature gradient in a
755 Mediterranean endemic coral. *Limnology and Oceanography*, 54(3), 930–937.
- 756 Goffredo, S., Prada, F., Caroselli, E., Capaccioni, B., Zaccanti, F., Pasquini, L., ... Falini, G.
757 (2014). Biomineralization control related to population density under ocean acidification.
758 *Nature Climate Change*, 4(7), 593–597. <https://doi.org/10.1038/NCLIMATE2241>
- 759 Hall-Spencer, J. M., Rodolfo-Metalpa, R., Martin, S., Ransome, E., Fine, M., Turner, S. M., ...
760 Buia, M. C. (2008). Volcanic carbon dioxide vents show ecosystem effects of ocean
761 acidification. *Nature*, 454(7200), 96–99. <https://doi.org/10.1038/nature07051>
- 762 Hennige, S. J., Wicks, L. C., Kamenos, N. A., Perna, G., Findlay, H. S., & Roberts, J. M. (2015).
763 Hidden impacts of ocean acidification to live and dead coral framework. *Proceeding Royal*
764 *Society B*, 282, 20150990. <https://doi.org/http://dx.doi.org/10.1098/rspb.2015.0990>
- 765 Hoffmann, A. A., & Sgro, C. M. (2011). Climate change and evolutionary adaptation. *Nature*,
766 470, 479–485. <https://doi.org/10.1038/nature09670>
- 767 Hofmann, G. E., Smith, J. E., Johnson, K. S., Send, U., Levin, L. A., Micheli, F., ... Martz, T. R.
768 (2011). High-frequency dynamics of ocean pH: A multi-ecosystem comparison. *PLoS ONE*,
769 6(12), e28983. <https://doi.org/10.1371/journal.pone.0028983>
- 770 Holcomb, M., Venn, A. A., Tambutté, E., Tambutté, S., Allemand, D., Trotter, J., & McCulloch,

- 771 M. (2014). Coral calcifying fluid pH dictates response to ocean acidification. *Scientific*
772 *Reports*, 4, 5207. <https://doi.org/10.1038/srep05207>
- 773 Kaniewska, P., Campbell, P. R., Kline, D. I., Rodriguez-Lanetty, M., Miller, D. J., Dove, S., &
774 Hoegh-Guldberg, O. (2012). Major cellular and physiological impacts of ocean acidification on
775 a reef building coral. *PLoS ONE*, 7(4), e34659. <https://doi.org/10.1371/journal.pone.0034659>
- 776 Kapsenberg, L., & Cyronak, T. (2019). Ocean acidification refugia in variable environments.
777 *Global Change Biology*, 00, 1–14. <https://doi.org/10.1111/gcb.14730>
- 778 Kersting, D. K., & Linares, C. (2019). Living evidence of a fossil survival strategy raises hope
779 for warming-affected corals. *Science Advances*, 5, eaax2950.
- 780 Kroeker, K. J., Bell, L. E., Donham, E. M., Hoshijima, U., Lummis, S., Toy, J. A., & Norton, E.
781 W. (2019). Ecological change in dynamic environments: Accounting for temporal
782 environmental variability in studies of ocean change biology, 00, 1–14.
783 <https://doi.org/10.1111/gcb.14868>
- 784 Kurihara, H., Takahashi, A., Reyes-Bermudez, A., & Hidaka, M. (2018). Intraspecific variation
785 in the response of the scleractinian coral *Acropora digitifera* to ocean acidification. *Marine*
786 *Biology*, 165(2), 38. <https://doi.org/10.1007/s00227-018-3295-1>
- 787 Kvitt, H., Kramarsky-Winter, E., Maor-Landaw, K., Zandbank, K., Kushmaro, A., Rosenfeld,
788 H., ... Tchernov, D. (2015). Breakdown of coral colonial form under reduced pH conditions is
789 initiated in polyps and mediated through apoptosis. *Proceedings of the National Academy of*
790 *Sciences of the United States of America*, 112(7), 2082–2086.
791 <https://doi.org/10.1073/pnas.1419621112>

- 792 Lough, J. M., & Barnes, D. J. (2000). Environmental controls on growth of the massive coral
793 Porites. *Journal of Experimental Marine Biology and Ecology*, 245, 225–243.
- 794 McCulloch, M., Falter, J., Trotter, J., & Montagna, P. (2012). Coral resilience to ocean
795 acidification and global warming through pH up-regulation. *Nature Climate Change*, 2(8),
796 623–627. <https://doi.org/10.1038/nclimate1473>
- 797 Mollica, N. R., Guo, W., Cohen, A. L., Huang, K. F., Foster, G. L., Donald, H. K., & Solow, A.
798 R. (2018). Ocean acidification affects coral growth by reducing skeletal density. *Proceedings*
799 *of the National Academy of Sciences of the United States of America*, 115(8), 1754–1759.
800 <https://doi.org/10.1073/pnas.1712806115>
- 801 Mouillot, D., Graham, N. A. J., Villéger, S., Mason, N. W. H., & Bellwood, D. R. (2013). A
802 functional approach reveals community responses to disturbances. *Trends in Ecology and*
803 *Evolution*, 28(3), 167–177. <https://doi.org/10.1016/j.tree.2012.10.004>
- 804 Movilla, J., Calvo, E., Coma, R., Serrano, E., López-Sanz, À., & Pelejero, C. (2016). Annual
805 response of two Mediterranean azooxanthellate temperate corals to low-pH and
806 high-temperature conditions. *Marine Biology*, 163, 135. [https://doi.org/10.1007/s00227-016-](https://doi.org/10.1007/s00227-016-2908-9)
807 2908-9
- 808 Palumbi, S. R., Barshis, D. J., Traylor-Knowles, N., & Bay, R. A. (2014). Mechanisms of reef
809 coral resistance to future climate change. *Science*, 344, 895–898.
810 <https://doi.org/10.1126/science.1251336>
- 811 Perez, S. O. (2015). Characterization of sodium potassium -ATPase and vacuolar proton -
812 ATPase in three coral species from two different clades. Thesis/dissertation. University of
813 California San Diego. Retrieved from <https://escholarship.org/uc/item/0xp4r2hb>

- 814 Prada, F., Caroselli, E., Mengoli, S., Brizi, L., Fantazzini, P., Capaccioni, B., ... Goffredo, S.
815 (2017). Ocean warming and acidification synergistically increase coral mortality. *Scientific*
816 *Reports*, 7, 40842. <https://doi.org/10.1038/srep40842>
- 817 Ries, J. (2011). Acid ocean cover up. *Nature Climate Change*, 1, 294–295.
- 818 Ries, J. B. (2011). A physicochemical framework for interpreting the biological calcification
819 response to CO₂ -induced ocean acidification. *Geochimica et Cosmochimica Acta*, 75(14),
820 4053–4064. <https://doi.org/10.1016/j.gca.2011.04.025>
- 821 Rodolfo-Metalpa, R., Houlbrèque, F., Tambutté, É., Boisson, F., Baggini, C., Patti, F. P., ...
822 Hall-Spencer, J. (2011). Coral and mollusc resistance to ocean acidification adversely affected
823 by warming. *Nature Climate Change*, 1(9), 1–5. <https://doi.org/10.1038/nclimate1200>
- 824 Savolainen, O., Lascoux, M., & Merilä, J. (2013). Ecological genomics of local adaptation.
825 *Nature Reviews Genetics*, 14(11), 807–820. <https://doi.org/10.1038/nrg3522>
- 826 Swain, T. D., Bold, E. C., Osborn, P. C., Baird, A. H., Westneat, M. W., Backman, V., &
827 Marcelino, L. A. (2018). Physiological integration of coral colonies is correlated with
828 bleaching resistance. *Marine Ecology Progress Series*, 586, 1–10.
829 <https://doi.org/10.3354/meps12445>
- 830 Takeshita, Y., Frieder, C. A., Martz, T. R., Ballard, J. R., Feely, R. A., Kram, S., ... Smith, J. E.
831 (2015). Including high frequency variability in coastal ocean acidification projections.
832 *Biogeosciences* (Vol. 12). <https://doi.org/10.5194/bgd-12-7125-2015>
- 833 Tambutté, E., Venn, A. A., Holcomb, M., Segonds, N., Techer, N., Zoccola, D., ... Tambutté, S.
834 (2015). Morphological plasticity of the coral skeleton under CO₂-driven seawater acidification.

- 835 *Nature Communications*, 6(7368), 1–9. <https://doi.org/10.1038/ncomms8368>
- 836 Teixidó, N., Gambi, M. C., Parravicini, V., Kroeker, K., Micheli, F., Villéger, S., & Ballesteros,
837 E. (2018). Functional biodiversity loss along natural CO₂ gradients. *Nature Communications*,
838 9, 5149. <https://doi.org/10.1038/s41467-018-07592-1>
- 839 Thomas, L., Rose, N. H., Bay, R. A., López, E. H., Morikawa, M. K., Ruiz-Jones, L., & Palumbi,
840 S. R. (2018). Mechanisms of thermal tolerance in reef-building corals across a fine-grained
841 environmental mosaic: lessons from Ofu, American Samoa. *Frontiers in Marine Science*, 4,
842 434. <https://doi.org/10.3389/fmars.2017.00434>
- 843 Tresguerres, M. (2016). Novel and potential physiological roles of vacuolar-type H⁺-ATPase in
844 marine organisms. *Journal of Experimental Biology*, 219(14), 2088–2097.
845 <https://doi.org/10.1242/jeb.128389>
- 846 Turner, J. S. (1973). *Buoyancy Effects in Fluids*. Cambridge University Press.
- 847 Zebral, Y. D., Da Silva Fonseca, J., Marques, J. A., & Bianchini, A. (2019). Carbonic anhydrase
848 as a biomarker of global and local impacts: Insights from calcifying animals. *International*
849 *Journal of Molecular Sciences*, 20(12), 1–16. <https://doi.org/10.3390/ijms20123092>
- 850 Zibrowius, H. (1995). The “southern” *Astroides calycularis* in the Pleistocene of the northern
851 Mediterranean—An indicator of climatic changes (Cnidaria, Scleractinia). *Geobios*, 28, 9–16.
- 852 Zoccola, D., Innocenti, A., Bertucci, A., Tambutté, E., Supuran, C. T., & Tambutté, S. (2016).
853 Coral carbonic anhydrases: Regulation by ocean acidification. *Marine Drugs*, 14, 109.
854 <https://doi.org/10.3390/md14060109>

855

ACKNOWLEDGEMENTS

We thank P. Sorvino (ANS Diving, Ischia), A. Passaretti and E. Di Meglio for their field assistance.

We also thank S. Durante (Rizzoli Orthopaedic Institute of Bologna) for assistance in performing computerized tomography scans and F. Italiano (National Institute of Geophysics and Volcanology) for the gas data. N.T. thanks M. Khamla for assistance in Figure 7 and E. Ferrer for

English grammar reviewing. **Funding:** This research was supported by the Total Foundation (High-CO₂ Seas grant, Grant No. BIO-2016-081-4), the French National Research Agency (4Oceans-MOPGA grant, ANR-17-MPGA-0001), and the ALMA IDEA (STRAMICRO grant, University of Bologna). N.T. was supported by a Maire Curie-Cofund (FP7-PEOPLE-Marie Curie Bandiera-Cofund, GA No. 600407) and by a Marie Skłodowska-Curie Global Fellowship under the European Union's Horizon 2020 research and innovation programme (H2020- MSCA- IF- 2015, GA No. 702628).

DATA AVAILABILITY STATEMENT

RNASeq FASTQ files for all 41 samples sequenced in this study were deposited in the NCBI Short Read Archive (SRA) under BioProject PRJNA643775 (Accession numbers SRR12135922 - SRR12135962), <https://dataview.ncbi.nlm.nih.gov/object/PRJNA643775?reviewer=5j14na61906tr4dne0bvg9kbhq>.

The de novo transcriptome assembly generated in this study and used for mapping the samples has been deposited in the NCBI Transcriptome Shotgun Assembly (TSA) database at DDBJ/ENA/GenBank under accession number GIRZ01000000 (<https://www.ncbi.nlm.nih.gov/nucleotide/GIRZ000000000>). The version described in this paper is the first version, GIRZ01000000. The bioinformatics scripts used for assembly, mapping, and SNP-calling are available on Github at DOI: 10.5281/zenodo.3934433.

879 AUTHOR CONTRIBUTIONS

880 N.T., E.C., S.P., E.S., S.G., M.C.G designed the study. N.T., E.C., S.A., S.C., F.M., A.M., M.M.,
881 S.P., E.S., L.U., C.d.V, M.C.G were involved with fieldwork. N.T., S.A., J.P.G., A.M., S.G.M.,
882 L.U., C.d.V. analyzed the environmental data; E.C., C.C., P.F., S.G. analyzed the skeletal data; E.
883 S., S. P., and N.T analyzed the genomic data. N.T. drafted the initial manuscript and all authors
884 contributed discussion, writing and interpretation.

885 COMPETING INTERESTS

886 The authors declare that they have no competing interests.

887 ETHICAL STATEMENT

888 All work undertaken in this study complied with current laws of Italy and United States of America
889 for collecting and importing/exporting coral specimens. Cites permits IT/EX/2018/MCE/00170,
890 IT/EX/2017/MCE/00214, IT/EX/2017/MCE/00325.

FIGURES AND TABLES

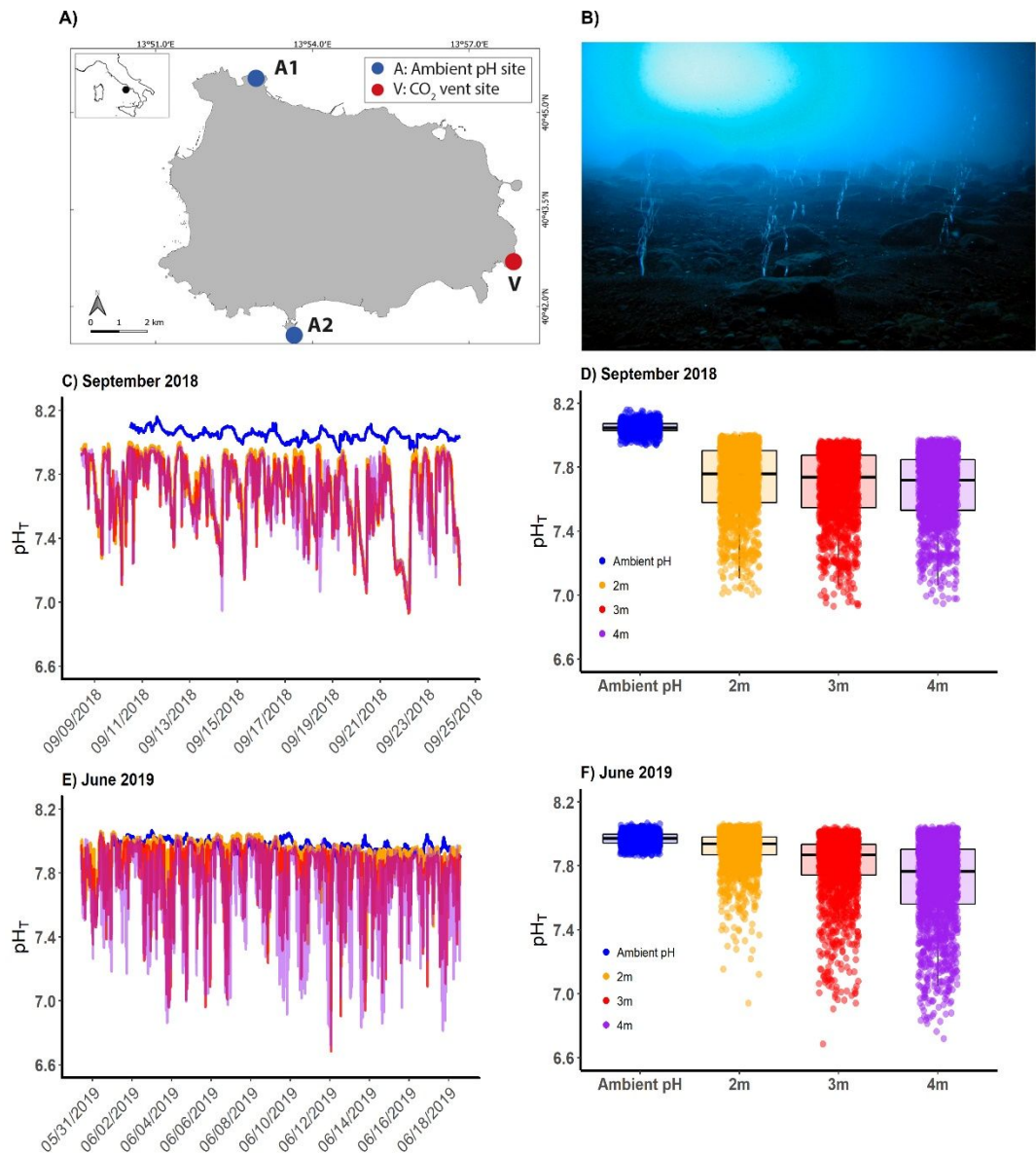


FIGURE 1. New CO₂ vent system and pH time series and variability. A) Map showing the location of the study sites along the coast of Ischia Island, Italy. V refers to the CO₂ vent system named *Grotta del Mago*: A1 (Ambient 1, Punta Vico) and A2 (Ambient 2, Sant'Angelo) are off-vent reference sites with ambient pH. B) The underwater volcanic vents occur in a semi-submerged cave at 5 m depth, release continuously gaseous emissions (92-95% CO₂, no sulfur), and do not

920 elevate temperature (Supporting Note 1, Figure S1, Tables S1, S5). C, E) Time series and D, F)
921 and pH_T (total scale) variability at the CO_2 vent site at 2 m (orange), 3 m (red), and 4 m (violet)
922 depth and at reference sites at 2 m with ambient pH (blue). Dates of pH_T series: from September 8
923 to September 24, 2018 ($n=1530$ for each depth at the CO_2 vent site and $n=1331$ for the ambient
924 pH site 1), and from May 30 to June 18, 2019 ($n=1840$ for each depth at the CO_2 vent site and $n=$
925 1691 for the ambient pH site 2). Measurements were taken every 15 minutes using SeaFETs
926 sensors.

927

For Review Only

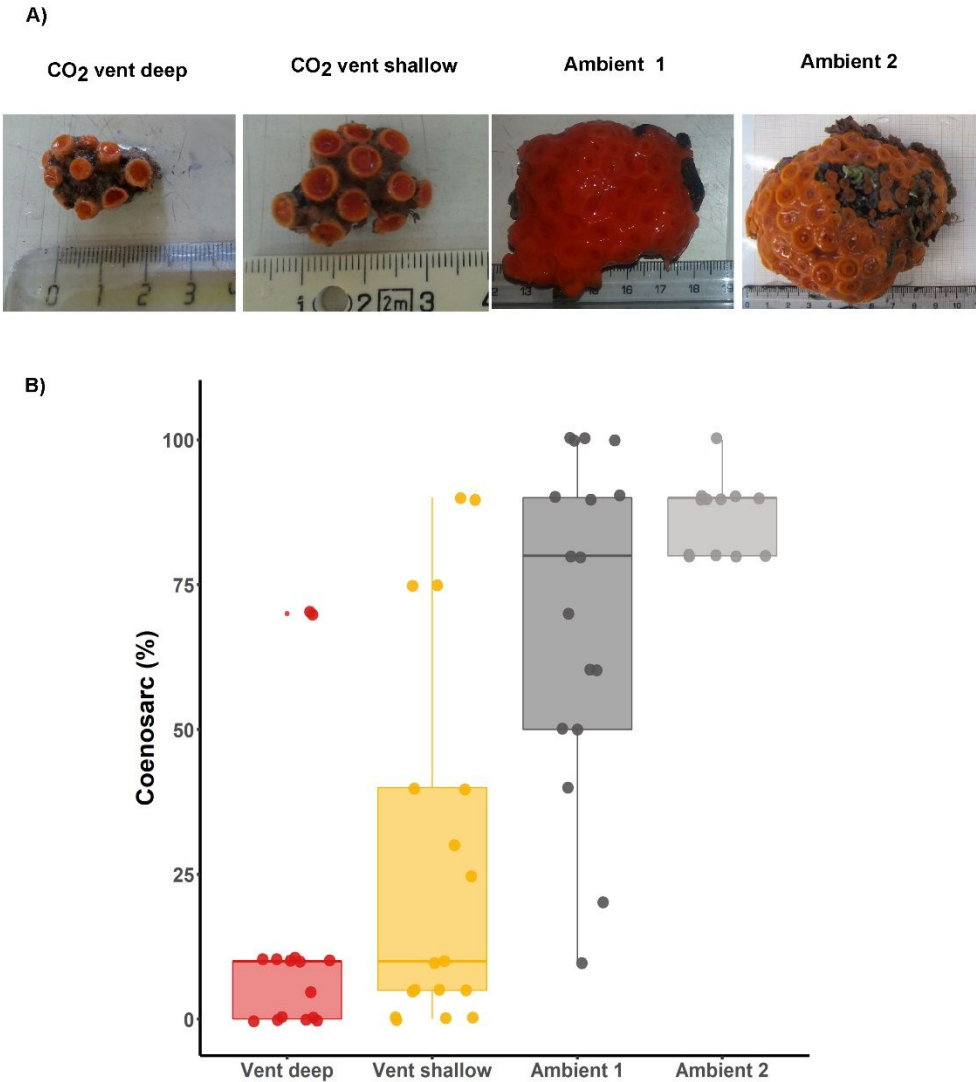


FIGURE 2. A) Photographs showing colonies sampled for skeletal characteristics and growth of the CO₂ vent system and off-vent reference sites with ambient pH. Vent system deep (3 m depth); Vent system shallow (1 – 2 m depth), Ambient 1= Punta Vico (1 – 2 m depth); Ambient 2 = Sant’Angelo (1 – 2 m depth). Colonies in the vent system exhibited encrusting form (flat growth form), whereas colonies in Ambient pH sites were a mixture of massive (extensive vertical and lateral growth) and encrusting forms (see also Figure S7). **B)** % Coenosarc (the living tissue connecting the polyps) of colonies among the study sites. Significant differences were found between vent (shallow and deep) and ambient pH populations ($F_{3,58} = 24.9$, $p < 0.0001$; pair-wise

950 comparisons between vent system deep -shallow and off-vent reference sites $p < 0.0001$). Number
951 of colonies = 66.

For Review Only

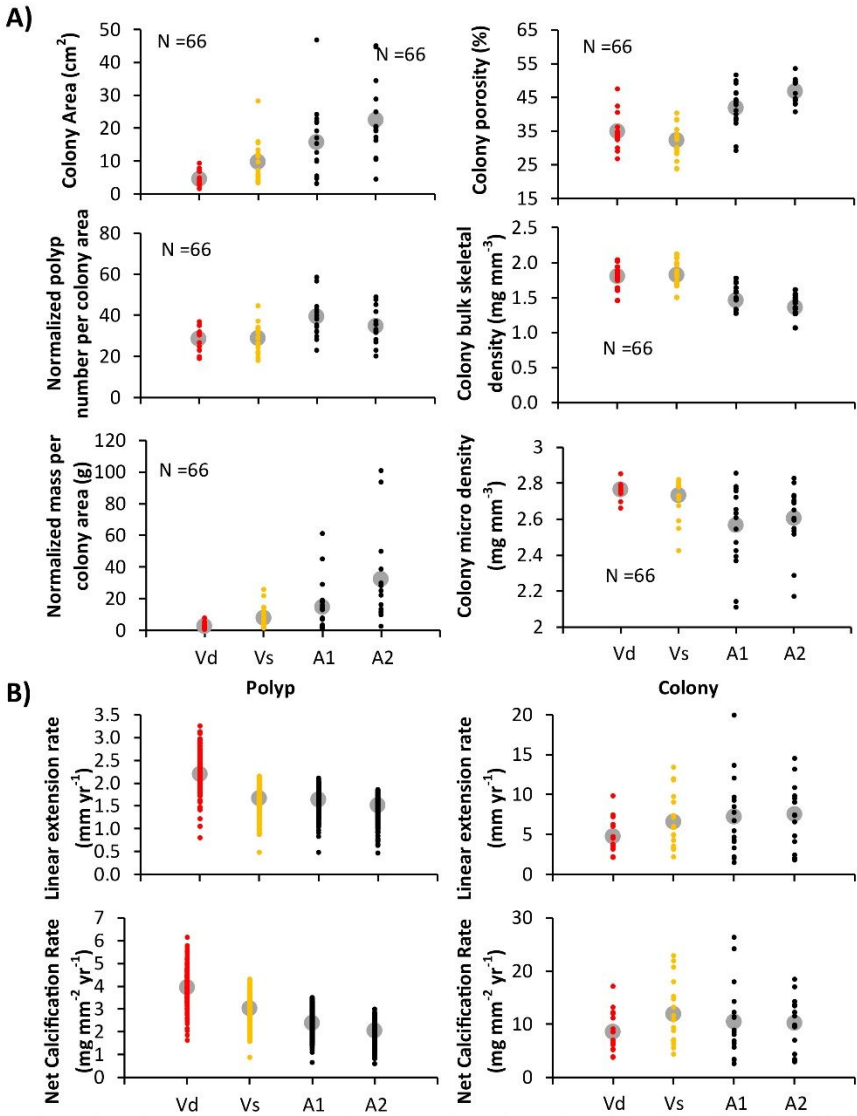


FIGURE 3. Skeletal and growth parameters measured in *A. calycularis*. **A)** Skeletal parameters of colonies and **B)** Growth parameters at polyp and colony levels at the CO₂ vent site (Vd and Vs) and ambient pH conditions (A1 and A2), respectively. Colony mass and polyp number were normalized to colony area. Grey circles in the plot represent the mean. Vd= Vent system deep, number of colonies =16; Vs= Vent system shallow, number of colonies = 18; A1= Ambient 1, number of colonies =17; A2 = Ambient 2, number of colonies = 15. Total number of colonies analyzed = 66.

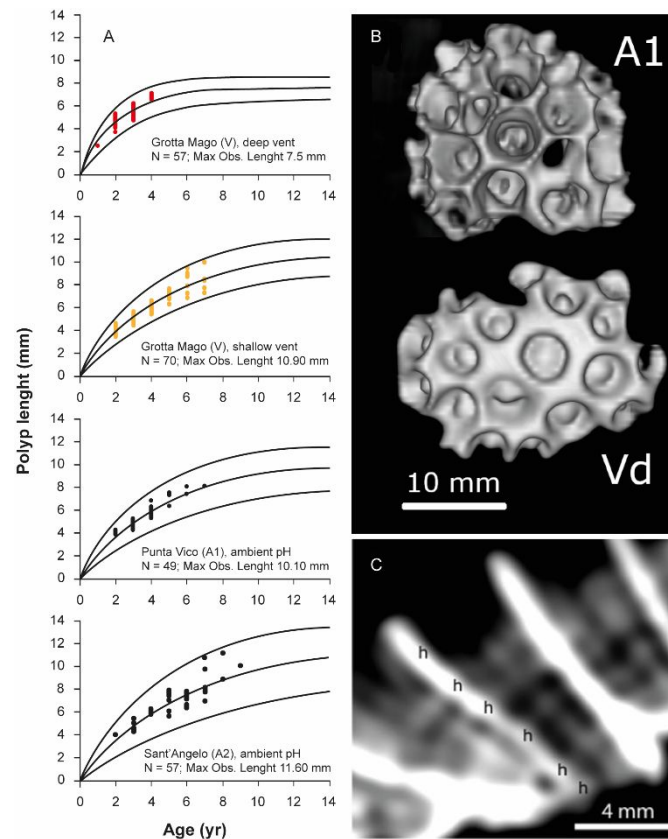
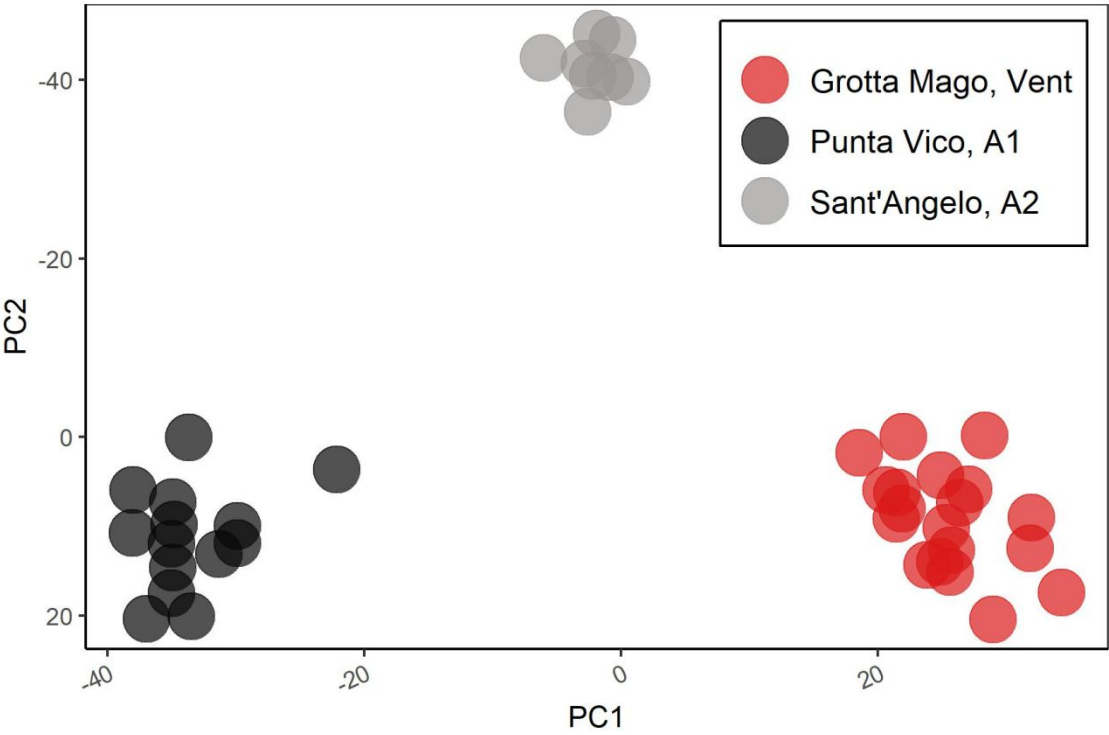


FIGURE 4. Relationships between age-length growth curves of *A. calycularis*. **A)** Age-length von Bertalanffy growth curves at the polyp (corallite) level. Dots indicate the age determined by counting the growth bands on computerized tomography. Lines indicate the mean von Bertalanffy growth curve and the 95% confidence interval). Values of L_{∞} (maximum expected length in the population) and K (a growth constant, larger for fast growth) were: 7.6 mm and 0.5 for Vent deep; 11.0 mm and 0.2 for Vent shallow; 10.2 mm and 0.2 for Ambient 1; and 11.8 mm and 0.17 for Ambient 2, respectively. **B)** Surface 3D rendering of the CT scans performed on a colony of *A. calycularis* from Ambient 1 (A1) and on another colony of similar surface area from Vent deep (Vd). Photograph of the deep vent (Vd) colony shows that same calcification is allocated to a minor number of polyps, and these few polyps result in having a more dense skeleton. **C)** Computerized tomography scan to count the growth bands on a single corallite. In this photograph, the corallite of *A. calycularis* is 6 years old; h indicates high density annual bands.

1004



1005

1006

1007

1008

1009

FIGURE 5. Population genetic structure of *A. calycularis* based on 46,784 single nucleotide polymorphisms (SNPs). Number of individuals: CO₂ vent site (Vent, Grotta Mago) = 19; ambient pH sites: Ambient 1 (A1, Punta Vico) = 14, Ambient 2 (A2, Sant' Angelo) = 8.

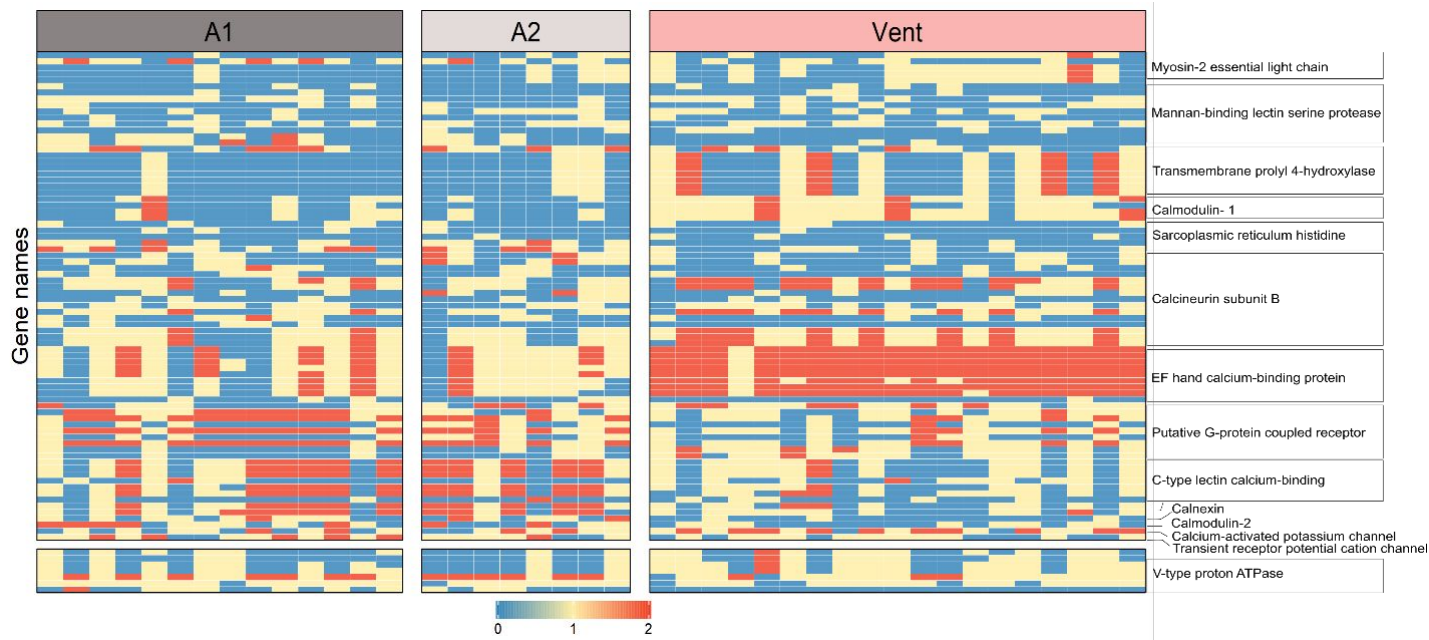


FIGURE 6. Upper: SNP genotypes for 13 calcium ion related loci showing high levels of divergence in the Grotta Mago population. Lower: Genotypes for 7 SNPs within a highly differentiated V-type proton ATPase potentially involved in pH regulation in the calcicoblastic layer where calcification occurs. Vent: CO₂ vent (Grotta Mago), A1: Ambient 1 (Punta Vico); A2: Ambient 2 (Sant'Angelo). Legend: 0 = homozygous major allele, 1 = heterozygous; 2 = homozygous minor allele.

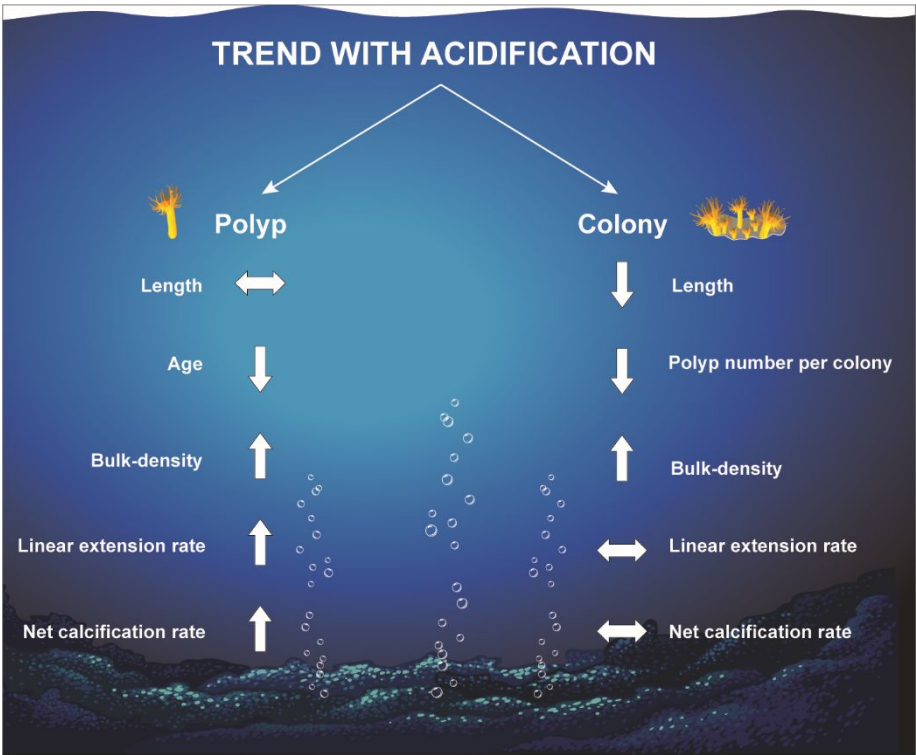


FIGURE 7. Schematic summary of the responses on skeletal and growth parameters to ocean acidification measured in the coral *A. calycularis* at the polyp and colony levels.

TABLE 1. Measured and estimated seawater physiochemical parameters at the CO₂ vent site and reference areas with ambient pH for salinity (S), temperature (T), total alkalinity (A_T), dissolved inorganic carbon (C_T), pH_T, pCO₂, calcite (Ω_c) and aragonite(Ω_a) saturation. Values are means, ± SD with 25th and 75th percentiles. Calculated concentrations of C_T, pCO₂, Ω_c and Ω_a are shown. 1: Parameters measured from discrete water samples; 2: parameters measured with *in situ* sensors. For detailed SeaFET pH sensor statistics and the carbonate system parameters, see Figure S5 and Table S5, respectively.

	Vent site (GM)			A1-PV	A2-SA
Month/year	2m	3 m	4 m	2 m	2 m
September 2018					
S	37.3 ¹ ± 0.2 (37.2, 37.5), n=9	37.3 ¹ ± 0.2 (37.2, 37.5), n=9	37.3 ¹ ± 0.2 (37.2, 37.5), n=9	37.3 ¹ ± 0 (37.3, 37.3), n=5	37.4 ¹ ± 0 (37.4, 37.4), n=3
T (°C)	25.9 ² ± 0.2 (25.8, 26.0), n=1530	26.0 ² ± 0.2 (25.8, 26.0), n=1530	26.0 ² ± 0.2 (25.9, 26.1), n=1530	17.3 ² ± 0.4 (17.0, 17.6), n=1331 ²	25.9 ² ± 0.2 (59.9, 26.1), n=408
A _T (μmol kg ⁻¹)	2564 ¹ ± 7 (2561, 2566), n=9	2562 ± 8 (2557, 2565), n=9	2562 ¹ ± 8 (2556, 2566), n=9	2618 ¹ ± 15 (2607, 2633), n=5	2610 ¹ ± 1 (2609, 2611), n=3
C _T (μmol kg ⁻¹)	2542 ± 79 (2477, 2585), n=1530	2552 ± 84 (2485, 2593), n=1530	2555 ± 80 (2495, 2598), n=1530	2262 ± 24 (2246, 2276), n=1331	2275 ± 1 (2275, 2276), n=3
pH _T	7.65 ² (7.58, 7.90), n=1530	7.62 ² (7.55, 7.87), n=1530	7.60 ² (7.53, 7.85), n=1530	8.05 ² (8.03, 8.07), n=1331	8.02 ¹ (8.02, 8.03), n=3
pCO ₂ (μatm)	2905 ± 1664 (1724, 3438), n=1530	3146 ± 1928 (1837, 3668), n=1530	3192 ± 1806 (1958, 3799), n=1530	322 ± 34 (298, 341), n=1331	375 ± 1 (374, 375), n=3
Ω _c	1.68 ± 0.59 (1.21, 2.21), n=1530	1.58 ± 0.56 (1.14, 2.09), n=1530	1.54 ± 0.54 (1.10, 1.98), n=1530	5.96 ± 0.36 (5.74, 6.21), n=1331	5.70 ± 0.01 (5.69, 5.70), n=3
Ω _a	1.11 ± 0.39 (0.80, 1.47), n=1530	1.05 ± 0.37 (0.75, 1.39), n=1530	1.02 ± 0.36 (0.73, 1.32), n=1530	3.86 ± 0.23 (3.72, 4.02), n=1331	3.71 ± 0.01 (3.70, 3.71), n=3
June 2019					
S	37.8 ¹ ± 0 (37.8, 37.8), n=7	37.8 ¹ ± 0 (37.8, 37.8), n=7	37.8 ¹ ± 0 (37.8, 37.8), n=7	38.0 ¹ ± 0 (38.0, 38.0), n=3	37.9 ¹ ± 0 (37.9, 37.9), n=7
T (°C)	21.9 ² ± 2.1 (19.9, 24.1), n=1840	21.8 ² ± 2.1 (19.8, 23.8), n=1840 ²	21.7 ² ± 2.0 (19.6, 23.4), n=1840 ²	26.2 ² ± 0.2 (26.1, 26.3), n=408	26.2 ² ± 1.1 (25.8, 27.0), n=1691 ²
A _T (μmol kg ⁻¹)	2539 ¹ ± 22 (2593, 2552), n=7	2541 ¹ ± 20 (2532, 2550), n=7	2551 ¹ ± 22 (2538, 2568), n=7	2630 ¹ ± 1 (2630.1, 2630.9), n=3	2642 ¹ ± 17 (2629, 2659), n= 7
C _T (μmol kg ⁻¹)	2450 ± 42 (2424, 2464), n=1840	2489 ± 75 (2443, 2509), n=1840	2535 ± 104 (2461, 2574), n=1840	2336 ± 3 (2320, 2353), n=3	2336 ± 23 (2320, 2353), n=1691
pH _T	7.88 ² (7.86, 7.98), n=1840	7.74 ² (7.74, 7.93), n=1840	7.60 ² (7.56, 7.90), n=1840	8.04 ¹ (8.04, 8.04), n=3	7.97 ² (7.94, 7.99), n=1691
pCO ₂ (μatm)	1531 ± 627 (1167, 1653), n=1840	2082 ± 1502 (1352, 2127), n=1840	2812 ± 2310 (1495, 3090), n=1840	372 ± 1 (372, 373), n=3	586 ± 76 (532, 635), n=1691
Ω _c	2.20 ± 0.41 (2.01, 2.46), n=1840	1.87 ± 0.54 (1.57, 2.26), n=1840	1.60 ± 0.65 (1.10, 2.14), n=1840	5.92 ± 0.01 (5.92, 5.93), n=3	5.34 ± 0.35 (5.08, 5.58), n=1691
Ω _a	1.44 ± 0.27 (1.32, 1.61), n=1840	1.23 ± 0.35 (1.03, 1.48), n=1840	1.05 ± 0.42 (0.72, 1.40), n=1840	3.89 ± 0.01 (3.86, 3.87), n=3	3.54 ± 0.23 (3.38, 3.71), n=1691

1045

1046